

Hadron Production and Phase Changes in Relativistic Heavy Ion Collisions

Jean Letessier^{1,2}, and Johann Rafelski^{1,2,3}

¹*Department of Physics, University of Arizona, Tucson, Arizona, 85721, USA*

²*Laboratoire de Physique Théorique et Hautes Energies
Université Paris 7, 2 place Jussieu, F-75251 Cedex 05 and*

³*CERN-Ph-Th, 1211 Geneva 23, Switzerland*

(Dated: April 8, 2005)

We study soft hadron production in relativistic heavy ion collisions in a wide range of reaction energy, $4.8 \text{ GeV} < \sqrt{s_{\text{NN}}} < 200 \text{ GeV}$, and make predictions about yields of particles using the statistical hadronization model. In fits to existent data, we obtain both statistical parameters as well as physical properties of the hadron source. We identify the properties of the fireball at the critical energy threshold, $6.26 \text{ GeV} < \sqrt{s_{\text{NN}}^{\text{cr}}} < 7.61 \text{ GeV}$, delineating for higher energies hadronization of an entropy rich phase. In terms of the chemical composition, one sees a phase which at low energy is chemically under-saturated, and which turns into a chemically over-saturated state persisting up to maximum accessible energy. Assuming then that there is no change in physical mechanisms in the energy range $15 > \sqrt{s_{\text{NN}}} \geq 200 \text{ GeV}$, we use continuity of particle yields and statistical parameters to predict the hadron production patterns at $\sqrt{s_{\text{NN}}} = 62.4 \text{ GeV}$, and to obtain total yields of hadrons at $\sqrt{s_{\text{NN}}} = 130$ and 200 GeV . We consider, in depth, the pattern we uncover within the hadronization condition, and discuss possible mechanisms associated with the identified rapid change in system properties at $\sqrt{s_{\text{NN}}^{\text{cr}}}$. We propose that the chemically over-saturated 2+1 flavor hadron matter system undergoes a 1st order phase transition.

PACS numbers: 24.10.Pa, 25.75.-q, 13.60.Rj, 12.38.Mh

I. INTRODUCTION

We present an analysis of the energy dependence of total hadron production yields for:

- fixed target symmetric Au–Au reactions at the top available AGS projectile energy 11.6 AGeV (energy per colliding nucleon pair $\sqrt{s_{\text{NN}}} = 4.84 \text{ GeV}$),
- fixed target symmetric Pb–Pb reactions at SPS at 20, 30, 40, 80 and 158 AGeV projectile energy. This we refer to as SPS energy range, $6.26 \leq \sqrt{s_{\text{NN}}} \leq 17.27 \text{ GeV}$,
- the Au–Au reactions in the collider mode at RHIC in $65+65$, $100+100$, and also at $31.2+31.2 \text{ AGeV}$ reactions for both total, and central rapidity yields. This is the RHIC energy range, $62.4 \leq \sqrt{s_{\text{NN}}} \leq 200 \text{ GeV}$.

As a first step, we aim to describe at each reaction energy the hadron yield data. We obtain in this process the statistical hadronization model (SHM) parameters, which allow to evaluate the yields of unobserved particles. One can see this as a method of how the experimental hadron yield data can be extrapolated to obtain the unobserved hadron yields. For this reason, we also attempt to extrapolate to reaction energies and phase space coverage which is not allowing for lack of data a SHM fit. For example, for the $31.2+31.2 \text{ AGeV}$ case, we interpolate strange particle yields known below and above this energy, and/or fix certain SHM parameters which show continuity as function of energy, respecting in the process the constraints of the SHM, in order to obtain both for central rapidity and full phase space coverage of soft hadron yields.

Once a statistically significant description of the data sample at an energy is achieved, we have available the yields of all soft hadronic particles and their resonances. We sum all partial contributions of each particle species

to quantities such as entropy, strangeness, baryon number, to obtain the properties of the fireball at the time of particle production (hadronization). In this way, we evaluate fireball breakup pressure, entropy, baryon number, strangeness yield and the thermal energy content. We note that, in this approach, the kinetic energy content associated with collective flow of matter is not considered — this requires a study of particle spectra not considered here.

It is believed that the deconfined phase of matter is formed at sufficiently high energy and reaction volume reached in the most central collisions of heavy ions at the top RHIC energy [1]. The question is where this critical energy threshold $\sqrt{s_{\text{NN}}^{\text{cr}}}$ is. We pursue this point in this systematic study, in order to explore possible phase changes occurring as function of collision energy [2], and compare our results qualitatively to the behavior seen as function of the reaction volume [3]. We are helped in this study of hadronic particles produced relatively late in the reaction history by the persistence of certain hadronic observables which carry important information about early stages of the collision process.

High strangeness [4], and entropy content [5, 6] of a dense hadronic matter fireball are the anticipated characteristic property of the color deconfined state of matter. Once formed, this enhancement of strangeness and entropy is also the property of the final hadronic state: first principles require that entropy must increase in the fireball expansion, as well as in the ensuing hadronization process; model studies show that once strangeness is produced, it remains present during expansion of dense matter, it can slightly increase during hadronization [7, 8].

Particle yields, and pion in particular, provide natural measure of entropy yield, while the kaon yields, and in

particular the K^+ yield, are an approximate measure of the total strangeness yield across all reaction energies [5]. The yield ratio K^+/π^+ has been studied as function of reaction energy in the SPS energy domain and a strong ‘horn’ like feature has been discovered [2].

This suggests a change in the reaction mechanism of particle production occurring, in most central collisions of Pb–Pb, in the energy interval $6.26 \text{ GeV} < \sqrt{s_{\text{NN}}} < 7.61 \text{ GeV}$, the two limits correspond to 20 and respectively, 30 AGeV/c Pb beams on fixed target. This energy range is just at the predicted threshold of quark–gluon formation arising considering balance of energy deposition and relativistic reaction dynamics [9]. Possibility of a rich phase structure of the deconfined phase at high baryochemical potential and finite temperature further enhances our interest in the study of this reaction energy domain [10].

To describe experimental results indicating the presence of a critical (‘cr’) energy threshold, one can, in first instance, use two different reaction models which apply below and, respectively, above a postulated energy threshold for a phase transformation [11]. However, this presupposes the most important outcome, namely that there is an energy dependent change in dense matter fireball structure at its breakup. Moreover, such an approach does not produce as result of analysis an insight into the structural change that occurs, and which could be compared with predictions. Instead, the structural change is part of the hypothesis under which the analysis is carried out. For this reason, the methodology we choose here is more general.

The tool, used in our study of soft hadron production, is the generalized statistical hadronization model (SHM) which allows for particle yields to be in chemical non-equilibrium. SHM is capable to describe in detail hadron abundances once the full mass spectrum of hadron resonances is included [12]. We use the software package SHARE (statistical hadronization with resonances) [13], the public SHM suit of programs, where the methods of SHM analysis are described in greater detail.

SHARE implements two features important for the full understanding of the K^+/π^+ horn:

- 1) the isospin asymmetry driven by proton-neutron asymmetry, which is particularly relevant at low reaction energies,
- 2) the chemical non-equilibrium (phase space under-saturation and over-saturation) for both strange and light quarks.

These two features appear to be essential to obtain a description of the K^+/π^+ energy dependent yield.

We first describe, in next section II, features of the data sample we use, discuss the input data and results of the fits for the AGS/SPS and RHIC energy range separately. We discuss the resulting statistical parameters and the confidence level of our fits. We survey in both tabular and graphic form the energy dependence of particle yields of interest, including an explanation of the K^+/π^+ horn. We then discuss physical properties of the

fireball at point of chemical freeze-out in section III, show the energy dependence of the model parameters and of physical properties, and address the strangeness and entropy production. We discuss the results of our analysis and draw conclusions in the final section IV.

II. FIT PROCEDURE AND HADRON MULTIPLICITIES

A. General remarks

The measured experimental results are available for either total particle yields, $N_{4\pi}$, or for central rapidity yields, dN/dy . At RHIC energy scale, we will study both data sets, though $N_{4\pi}$ is rather incomplete at this time. At SPS and AGS we will solely consider $N_{4\pi}$, in order to minimize the impact of the shape of the longitudinal unstopped matter flow on the outcome of the analysis.

At SPS, a semi-distinct central rapidity domain is only present in the top SPS case, its re-analysis will make good sense once the RHIC dN/dy data extend to the minimum accessible energy domain which is close to top SPS energy range. However, this will require introduction of models of collective matter flow, a step which we do not wish to take in this work. At high RHIC energies, we presume that the fragmentation regions are sufficiently separated from the central rapidity domain as to allow the study of the rapidity particle distributions dN/dy , at central rapidity, in a model independent fashion.

We include in our consideration of the total particle yields $N_{4\pi}$ the trigger condition which defines the participant ‘wounded’ nucleon number N_W . This has to be equal to the total net baryon number b contained within the final state particle multiplicities. Furthermore, both for $N_{4\pi}$ and central rapidity yields dN/dy , we consider two constraints:

- a) the fraction of protons among all nucleons (0.39 for heavy nuclei) establishes a fixed final ratio of all electrical charge Q to the total final state baryon number b ;
- b) strangeness content of hadrons prior to weak decays has to be balanced by antistrangeness bound in hadrons, exactly for $N_{4\pi}$ study, and nearly exactly when considering the central rapidity dN/dy distributions.

As our prior studies showed [14], any deviation from strangeness conservation as function of rapidity is, in general, considerably smaller than the typical 10% precision of the experimental data points. However, even for the $N_{4\pi}$ results, we do not think that the *exact* strangeness conservation should be always insisted on. This can create an aberration of the fit, since the sharp constraint is inconsistent with several independent measurements which contribute to the cancellation, which have statistical and systematic errors at 10% level. Clearly, sometimes, it is impossible to balance strangeness exactly. This can be checked without a fit in a qualitative study of the key particle yields. This has to happen seen the amount of data we process.

Another reason to be cautious with the strangeness conservation is that the spectra of hadrons we are using could contain wrong entries (e.g., pentaquark states which we include in the input data set, or wrong spin-isospin assignments for little known states). Moreover, we maybe missing some relevant undiscovered resonances. These effects are largest when the baryon asymmetry is largest, since the strangeness balance condition probes for at large baryochemical potential the mass spectrum of strange baryons and mesons separately, and asymmetrically.

For this reason, our strangeness conservation procedure is further amended as follows: when a fit prefers a slight strangeness asymmetry, we find the best parameters for the fit with a loose strangeness conservation constraint allowing, e.g., a 10% deviation from balance. We fix the preferred value of one of the parameters (typically strangeness fugacity λ_s) as is done in case of using exact strangeness conservation. We then refit with this fixed value. In this way, we obtain a data fit with the same mechanism of approach as for the cases where strangeness conservation is naturally present, and as it were used to fix one parameter. We employ this procedure for 40 and 80 A GeV cases. We find $-0.07 > (s-\bar{s})/(s+\bar{s}) > -0.09$. The asymmetry favors overcount of \bar{s} quarks in emitted hadrons. It is moderate in its relative magnitude, staying within the systematic errors of the measurements used in this study. We will state the strangeness balance explicitly when presenting the computed particle yields.

As the above discussion of strangeness conservation shows, there are significant consistency constraints arising from conserved quark quantum number considerations, which particle multiplicities cannot deviate from. How a subset of SHM parameters determine a set of particle ratios has been shown for the first time in 1982 [15]. A nice example is the chemical relation between the K^-/K^+ and \bar{p}/p demonstrated experimentally in 2003, see figure 4 in [16], a development based on the rediscovery of the SHM constraints in 2000 [17]. Since SHM with its chemical consistencies has been very successful in helping understand hadron production, we embark on further data verifications at each energy, checking the consistency of experimental data with SHM. We follow this path to be sure that no single particle yield can materially alter the analysis and influence the outcome of our study.

A suspect particle yield effect can be further cross checked studying the behavior of this particle yield as function of energy. Such consideration is very important since we are searching for a change in the physical properties of the fireball as function of energy, and we do not want the outcome to be even in part the result of a statistical fluctuation in the reported yield of particles. We find inconsistencies in the particle yield effects at the level of up to 2 s.d. in such consideration. None of these influence decisively the findings we report here, in part because of the more lax attitude we take toward the constraint on strangeness conservation we described above.

Moreover, considering the large number of data considered, fluctuations in experimental data sample must occur. Therefore, we will not pursue these in a more detailed discussion here. The interested reader can recognize these cases by comparing the output multiplicities obtained with the input multiplicity data tables, and in some cases, see it in the multiplicity figures.

B. AGS and SPS energy range fit

To assure the reproducibility of our analysis, we will describe in detail the input particle yields that are used, for AGS/SPS energy domain, and for RHIC domain in the next subsection. The set of particles available at AGS arises from several experiments, we have previously reported in detail the SHM analysis at the top AGS energy [18], which input and fit results are restated here. Differences in detail yield similar fit result and show the robustness of the approach.

For this work, the analysis of the $N_{4\pi}$ particle yields of the NA49 experimental group available at 20, 30, 40, 80 and 158 A GeV [2, 19, 20] has been carried out. This work extends significantly our prior study of the 40, 80 and 158 A GeV NA49 done when many fewer measurements were available [21]. Moreover, the SHARE package used offers additional theoretical features which were not available earlier. The difference to the earlier study is that we can address the two newly measured reaction energies, 20, 30 A GeV. This, along with the AGS 11.6 A GeV data, including the recently published ϕ -yield [22], allows to recognize a major change in the behavior of the hadronizing fireball [2].

The input data we considered for the AGS and SPS are presented in top part of the table I. The statistical parameters are seen below these input data. In carrying out the data analysis, we use the full grand-canonical statistical set of seven parameters: volume V , freeze-out temperature T , chemical quark fugacities $\lambda_{q,s}$, quark occupancy parameters γ_q and γ_s , and third component of the isospin fugacity λ_{I3} . The fitted values of these 7 parameters are seen near bottom of the table I, which is followed by entries for the central values of the two chemical potentials:

$$\mu_B = 3T \ln \lambda_q, \quad (1)$$

$$\mu_S = \mu_B/3 - T \ln \lambda_s. \quad (2)$$

The uncertainties in the value of statistical parameters comprise the propagation of experimental measurement error through the fit, as well as ambiguity due to statistical parameter correlations arising. In some instances this effect is very small, in others rather large. This wide disparity is possible, as sometimes the data set is sufficiently constraining, and in others it is not. The most interesting result we notice in table I is the sudden shift in the values of the phase space occupancies observed as reaction energy rises from 20 to 30 A GeV. The value of

TABLE I: The input $N_{4\pi}$ total particle multiplicities data at top, and the resulting statistical parameters for AGS and CERN energy range. For each projectile energy E [AGeV], we also present in the header the invariant center of momentum energy per nucleon pair, $\sqrt{s_{NN}}$ [GeV], the center of momentum rapidity and the centrality of the reaction considered. The λ_s values marked with a * are result of a strangeness conservation constraint. At bottom, we state the chemical potential corresponding to the central values of the fugacities.

E [AGeV]	11.6	20	30	40	80	158
$\sqrt{s_{NN}}$ [GeV]	4.84	6.26	7.61	8.76	12.32	17.27
y_{CM}	1.6	1.88	2.08	2.22	2.57	2.91
$N_{4\pi}$ centrality	most central	7%	7%	7%	7%	5%
$R = p/\pi^+, N_W$	$R = 1.23 \pm 0.13$	349 ± 6	349 ± 6	349 ± 6	349 ± 6	362 ± 6
Q/b	0.39 ± 0.02	0.394 ± 0.02	0.394 ± 0.02	0.394 ± 0.02	0.394 ± 0.02	0.39 ± 0.02
π^+	133.7 ± 9.9	184.5 ± 13.6	239 ± 17.7	293 ± 18	446 ± 27	619 ± 48
$R = \pi^-/\pi^+, \pi^-$	$R = 1.23 \pm 0.07$	217.5 ± 15.6	275 ± 19.7	322 ± 19	474 ± 28	639 ± 48
$R = K^+/K^-, K^+$	$R = 5.23 \pm 0.5$	40 ± 2.8	55.3 ± 4.4	59.1 ± 4.9	76.9 ± 6	103 ± 10
K^-	3.76 ± 0.47	10.4 ± 0.62	16.1 ± 1	19.2 ± 1.5	32.4 ± 2.2	51.9 ± 4.9
$R = \phi/K^+, \phi$	$R = 0.025 \pm 0.006$	1.8 ± 0.4	1.73 ± 0.2	2.57 ± 0.2	4.58 ± 0.7	7.6 ± 1.1
Λ	18.1 ± 1.9	28 ± 1.5	41.9 ± 6.1	43.0 ± 6.9	44.7 ± 6.0	44.9 ± 8.9
$\bar{\Lambda}$	0.017 ± 0.005	0.16 ± 0.03	0.50 ± 0.04	0.66 ± 0.14	2.02 ± 0.45	3.74 ± 0.62
Ξ^-				2.41 ± 0.39		4.45 ± 0.22
Ξ^+						0.83 ± 0.04
$\Omega + \bar{\Omega}$				0.12 ± 0.07		
K_S						81 ± 4
V [fm ³]	3380 ± 381	5378 ± 291	1982 ± 347	2092 ± 747	2665 ± 294	3676 ± 751
T [MeV]	161 ± 5	158 ± 10	123 ± 3	130 ± 7	135.5 ± 9	134.3 ± 11
λ_q	5.29 ± 1.46	3.48 ± 0.87	2.70 ± 0.1	2.34 ± 0.21	1.91 ± 0.07	1.72 ± 0.12
λ_s	1.567^*	1.41^*	1.42^*	1.28^*	1.21^*	1.16^*
γ_q	0.315 ± 0.27	0.41 ± 0.20	1.706 ± 0.006	1.6^*	1.648^*	$1.64^{+0.01}_{-0.5}$
γ_s	0.18 ± 0.11	0.31 ± 0.07	1.68 ± 0.17	1.42 ± 0.22	1.39 ± 0.2	1.46 ± 0.8
λ_{T3}	0.875 ± 0.04	0.89 ± 0.03	0.935 ± 0.006	0.937 ± 0.026	0.955 ± 0.016	0.962 ± 0.023
μ_B [MeV]	807	592	367	332	260	218
μ_S [MeV]	197	142	79.4	78.5	61.5	53.0

chemical freeze-out temperature changes accordingly to counterbalance this effect on some particle multiplicities. We will discuss this change in behavior in great detail in what follows. The steady decrease of baryochemical potential μ_B with reaction energy follows the expectation that there is steady increase of baryon transparency with increasing collision energy. The associated value of μ_S is controlled by strangeness conservation condition.

Considering the implicit (not stated in the table) strangeness conservation constraint, there are between 11 and 13 data inputs and constraints at each energy considered in table I, and up to 7 parameters. We thus have 3–5 degrees of freedom (d.o.f) for the fits carried out at AGS and SPS. Not all of the NA49 SPS energy range results we use are published in final form. As seen in table I, we occasionally fix the value of γ_q . The value we choose is the the best value which emerges from study of χ^2 profile, see figure 1. This step is made to reduce the correlations between parameters, given the small number of degrees of freedom.

We show, in figure 1, the reliability of the fits we obtained at different reaction energies as function of γ_q , the light quark phase space occupancy. The results for AGS and SPS are accompanied by those for central rapidity RHIC fits we will address below. The top frame, in figure 1, shows χ^2/dof . The associated significance level $P[\%]$

is seen in the bottom frame. We include $P[\%]$ as result, since the number of degrees of freedom in each fit is small and it is hard to judge the significance of a small value of χ^2/dof .

We study dependence of χ^2/dof and $P[\%]$ on γ_q , since we see in table I that the two parameters which undergo a rapid change as function of reaction energy are γ_q , and to a lesser degree, the freeze-out temperature T . The rapid change with γ_q is prominent in figure 1 where $P[\%]$ peaks for the lowest two energies (11.6 and 20 AGeV) at $\gamma_q < 0.5$, while for all other collision energies it grows to maximum value near $\gamma_q \simeq 1.6$, where the Bose singularity of the pion momentum distribution $\gamma_q \simeq e^{m_\pi/T}$.

The reader will can see, in figure 1, that setting the value $\gamma_q = 1$ will yield a set of energy dependent *individual* fits which appear to have a good confidence level. However, the energy dependence of the particle yields is less convincing in this case. It is the rapid shift in the best γ_q as function of reaction energy which allows to describe the ‘horn’ feature in the K^+/π^+ data (see below figure 2). Without variable γ_i this horn feature is largely erased, see, e.g., figure 4 in [23], and the dashed and dotted lines in figure 2. We will discuss this phenomenon in more detail in section IV A. We believe that, in the study of energy dependent particle yields, the full power

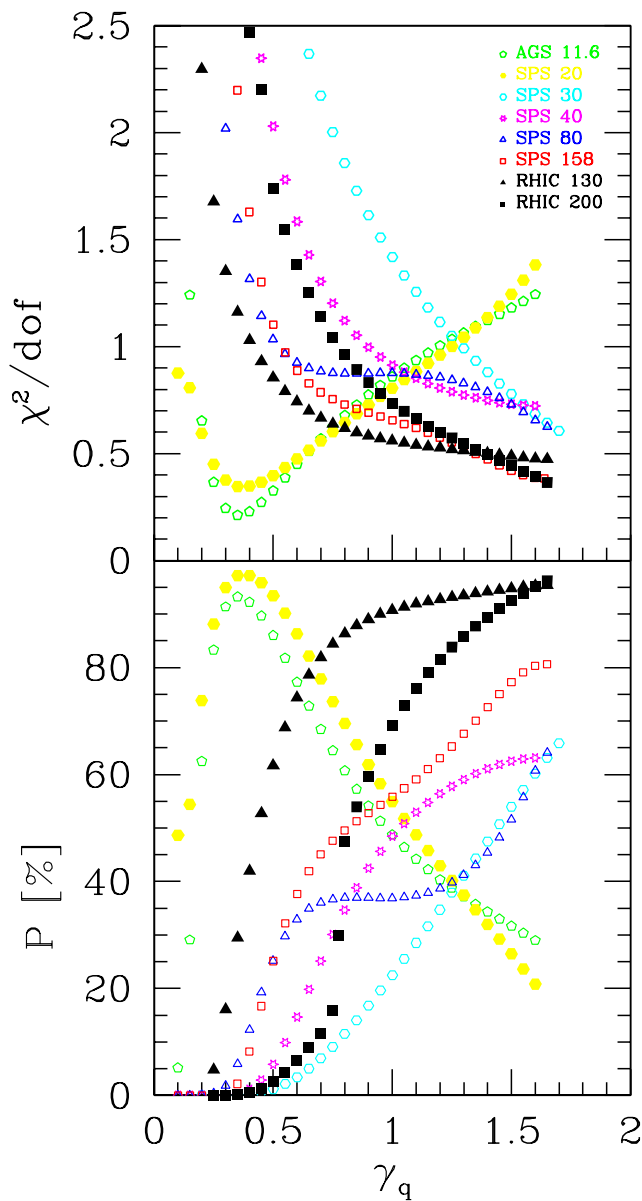


FIG. 1: χ^2/dof (top) and the associated significance level P [%] (bottom) as function of γ_q , the light quark phase space occupancy, for the AGS/SPS energy range and for the (central rapidity) RHIC results.

of the method SHM with $\gamma_i \neq 1$ is required to arrive at a valid understanding of the data.

Regarding the weak decay (WD) contributions:

- we always include by default the decay products of $\Sigma^\pm \rightarrow \pi N$;
- pion yields are nearly always fully corrected and do not include the WD contributions.

The other WD corrections are variable and depend on the corrections applied to the data by the experimental group. In the data we use for SPS, the decay of hyperons into nucleons is of relevance. For 20 and 30 GeV in Λ and $\bar{\Lambda}$, the data we use includes the WD contributions

TABLE II: Output total hadron multiplicity data for AGS (left) and SPS (right). Additional significant digits are presented in particle yields for purposes of tests and verification. The statistical parameters generating these multiplicities are the central fit values seen in table I. Nucleons from weak decay of hyperons are included at 20 and 30 A GeV, see text for further discussion. All results presented are the total multiplicities $N_{4\pi}$ expected at the most central collision bin. For SHM parameters, see table I.

E [A GeV]	11.6	20	30	40	80	158
$\sqrt{s_{\text{NN}}}$ [GeV]	4.84	6.26	7.61	8.76	12.32	17.27
y_{CM}	1.6	1.88	2.08	2.22	2.57	2.91
$N_{4\pi}$ centrality	m.c.	7%	7%	7%	7%	5%
$b \equiv B - \bar{B}$	383.2	348.5	349.5	349.6	349.8	361.9
π^+	134.5	187.0	240.7	284.4	429.3	594.9
π^-	163.0	219.5	277.9	324.2	472.0	647.1
K^+	17.4	39.2	51.5	58.9	78.4	109.3
K^-	3.57	10.3	16.1	20.1	34.4	51.9
K_S	10.8	25.2	33.7	39.4	55.8	80.4
ϕ	0.47	1.74	1.92	2.48	3.94	6.32
p	177.0	163.9	162.2	136.6	139.3	145.5
\bar{p}	0.022	0.214	0.74	0.90	3.01	5.98
Λ	18.5	28.6	37.1	32.5	37.0	43.7
$\bar{\Lambda}$	0.017	0.16	0.49	0.67	1.93	3.82
Ξ^-	0.57	1.48	2.56	2.60	3.35	4.47
Ξ^+	0.0033	0.030	0.085	0.171	0.42	0.83
Ω	0.013	0.059	0.12	0.124	0.18	0.28
$\bar{\Omega}$	0.0009	0.0074	0.015	0.028	0.059	0.12
$K^0(892)$	6.08	13.38	9.60	12.7	18.0	25.2
Δ^0	39.7	33.68	24.0	26.1	26.8	27.8
Δ^{++}	31.2	27.13	21.2	23.1	24.6	25.9
$\Lambda(1520)$	1.41	2.04	1.59	1.83	2.21	2.63
$\Sigma^-(1385)$	2.55	3.74	3.78	4.05	4.61	5.42
$\Xi^0(1530)$	0.16	0.40	0.61	0.65	0.86	1.16
η	7.26	15.6	19.2	23.5	36.0	53.2
η'	0.34	1.07	1.02	1.39	2.26	3.48
ρ^0	16	24	15	22	34.5	48
$\omega(782)$	6.04	14.4	11.5	17.0	29.9	41.2
$f_0(980)$	0.32	0.964	0.86	1.21	2.00	3.03
$\Theta^+(1540)$	0.566	0.773	6.56	6.01	5.72	5.87
$(s - \bar{s})/(s + \bar{s})$	0	0	0	-0.085	-0.072	0

by hyperon decays, at all higher SPS energies these have been corrected in data and we do not introduce the WD contributions. At AGS 11 GeV, all yields we consider are without WD contribution. The contamination of Λ by hyperons decays is not material. In the presentation of particle multiplicities in table II, the same WD pattern is followed.

The model yields obtained are shown in table II. We present there also the input particles can be compared to the fitted inputs seen in table I. We present also predictions for yields of other particles of interest. We do not show the uncertainty in these results, which can be considerable: in addition to the error propagating through the fit, there is systematic error due to the shape of the $\chi^2/\text{d.o.f.}$ minimum, seen figure 1.

A novel and interesting observable is the recently pro-

posed pentaquark state $\Theta^+(1540)[uudd\bar{s}]$. It is highly sensitive to the hadronization conditions [24]. We see that the expected statistical hadronization yield rises by factor 8 in the threshold energy range considered. As we see, the expected $\Theta^+(1540)$ yield is largest at 30 A GeV and the background multiplicity lowest, and the rapidity range very restricted compared to the top SPS energy. Thus, we hope and expect that reactions at this energy (30 A GeV) will demonstrate convincingly the existence or non-existence of this new state. It should be noted that the expected production of $\Theta^+(1540)$ exceeds the predicted yield of $\Lambda(1520)$ by a factor 4 at this energy.

We did not use the $\Lambda(1520)$ yield in our fit. The preliminary value at top SPS energy 158 A is $\Lambda(1520) = 1.4 \pm 0.4$ [25]. This is within 2s.d. of the predicted value. However, this exceptionally narrow resonance may be subject to additional effects [26] and we felt that it is more prudent to not include its study here.

C. RHIC energy range fit

The RHIC central rapidity particle yields at $\sqrt{s_{\text{NN}}} = 200$ and 130 GeV are analyzed using nearly the same method and principles described in the study of the total particle yields. This can be done for the case that the particle yields, and hence their source, is subject to scaling, that means is flat as function of the rapidity distribution [27]. The overall normalization of yields then contains, instead of the volume V , the volume fraction dV/dy associated with the size of the volume at the rapidity of the source of particles at y . We note that, in the local rest-frame, the total yield of particles $N_{4\pi}$ can be written in the equivalent forms:

$$N_{4\pi} = \int dV \rho = \int dy \frac{dV}{dy} \rho = \int dy \frac{dN}{dy}. \quad (3)$$

The local rest frame particle density, $\rho = dN/dV$, is thus related to the rapidity density by

$$\frac{dN}{dy} = \frac{dV}{dy} \rho. \quad (4)$$

The SHM fits to particle densities dN/dy thus produce as the normalization factor the value dV/dy . The qualitative relation between dV/dy and V (rest-frame hadronization volume) must include the maximum rapidity range $2y_p$, where y_p is the rapidity of the nuclei colliding head on,

$$V = k \frac{dV}{dy} \times 2y_p, \quad (5)$$

where k is a reaction energy dependent constant, the study of the total hadron yields at RHIC we present suggests $k \simeq 0.4$ – 0.6 .

A study of the impact parameter dependence of central rapidity particle multiplicities dN/dy at $\sqrt{s_{\text{NN}}} = 200$ GeV has been carried out [3]. These results for the the

most central 5% events are recovered here for the experimental input data seen in the top section, in table III, in right most column, for the source of these experimental data see Ref.[28–31]. Regarding the weak decays, those of Σ^\pm are assume to be always fully accepted, as are, due to the short lifespan of the K_S these decay products. When we accept mesons from hyperon decays we also accept 10% of K_L decay products. We fit here the WD *uncorrected* yields of p and \bar{p} obtained from the WD uncorrected hadron ratios given in Ref.[28], table IX: $\bar{p}/p = 0.747 \pm 0.53$, $p/\pi^+ = 0.099 \pm 0.007$, $\bar{p}/\pi^- = 0.075 \pm 0.005$. The entries in table III for p and \bar{p} and in table IV for nucleons and hyperons are the yields including all baryons from hyperon decays but excluding the mesons from hyperon decays.

We proceed in this way since a reanalysis of the $\sqrt{s_{\text{NN}}} = 200$ GeV has been carried out recently [32]. This work comprises a study of the hyperon weak decay contamination of p and \bar{p} within the SHM. These turn out to be somewhat larger than used by the PHENIX collaboration. The fully corrected p and \bar{p} within the SHM are reduced, compared to PHENIX, by 1s.d. and 1.5s.d., respectively, and are $p = 15.7 \pm 2.6$ (down from 18.4 ± 2.6) and $\bar{p} = 11.0 \pm 1.8$ (down from 13.5 ± 1.8).

The $\sqrt{s_{\text{NN}}} = 130$ GeV experimental results (second column from right in the top section of table III), are drawn from several sources, see Ref.[33–40]. For the fits of dN/dy at $\sqrt{s_{\text{NN}}} = 130$ and 200 GeV, we present the quality of the fit results in figure 1 (black triangles and squares, respectively). The mesons and baryons are fed by WD as discussed for the case of $\sqrt{s_{\text{NN}}} = 200$ GeV, in particular here, accepting the hyperon decays.

We can expect, in near future, particle multiplicity results from RHIC obtained at $\sqrt{s_{\text{NN}}} = 62.4$ GeV. We interpolate the central rapidity yields of strange hyperons $\Lambda, \bar{\Lambda}, \Xi$ and $\bar{\Xi}$, presented in [41], to this energy. With these 4 inputs, two constraints, setting the $\gamma_s = \gamma_q = 1.64$, $T = 140$ and choosing $dV/dy = 1500 \text{ fm}^3$, we obtain a good description of the interpolated data with quite a few degrees of freedom. We have four interpolated ‘data’ points, two constraints — strangeness conservation and Q/b , thus 6 data points which are fitted using two flexible parameters, λ_q and λ_{I3} . This set of parameters, then, yields our prediction of central rapidity particle multiplicities seen in table IV for $\sqrt{s_{\text{NN}}} = 62.4$ GeV.

We make an effort to understand also the recently finalized total multiplicities $N_{4\pi}$ of K^\pm and π^\pm [42] at $\sqrt{s_{\text{NN}}} = 200$ GeV. Additional qualitative constraint is derived from total charge particle multiplicities [43], however this result is not used directly in the fit. With the three constraints, four BRAHMS particle yields, we have 7 data points, and also 7 SHM parameters. To be able to make a fit with at least one degree of freedom it is necessary to make some ‘natural’ hypothesis. We choose to consider $\gamma_q \simeq e^{m_\pi/2T}$, which we find systematically at the RHIC energy scale. Our ‘fit’ to $N_{4\pi}$ data $\sqrt{s_{\text{NN}}} = 200$ GeV works, but it must not be seen as a fit, rather a con-

TABLE III: The input particle data (top) and the resulting statistical parameters, and the chemical potentials derived from these, at bottom, for the RHIC energy range. Any of the entries with a * is set as input or is a constraint, e.g., in general λ_s results from the constraint to zero strangeness. † indicates input particle multiplicity derived from interpolating yields between different energies, applies in particular to the RHIC $\sqrt{s_{NN}} = 62.4$ GeV case. On right, the case of central rapidity yields dN/dy , and on left, the total particle yields, in all cases considered for the most central 7% collisions. For $N_{4\pi}$, we show the participant count.

$\sqrt{s_{NN}}$ [GeV]	62.4	130	200	62.4	130	200
E_{eq} [A GeV]	2075	9008	21321	2075	9008	21321
Δy	± 4.2	± 4.93	± 5.36	± 4.2	± 4.93	± 5.36
	$N_{4\pi}$ 5%			$dN/dy _{y=0}$ 5%		
N_W	349±6	349±6	349±6			
Q/b	0.39±0.02	0.39±0.02	0.39±0.02	0.39±0.02	0.4±0.01	0.4±0.01
π^-/π^+					1±0.02	1.01±0.02
π^+	†1140±90	†1459±90	1677±150			
π^-			1695±150		239±14	281.8±22.8
K^+			293±29		48±7	48.9±6.3
K^-			243±22		43.5±6	45.7±5.2
ϕ/K^-					0.15±0.03	0.16±0.03
p						28.3±4.8
\bar{p}						20.8±3.4
\bar{p}/p					0.71±0.06	
K^+/p					2.4±0.5	
Λ				†17±2	17.3±1.8	
$\bar{\Lambda}$				†10±1	12.7±1.8	
Ξ^-/Λ					0.187±0.046	
$\Xi^+/\bar{\Lambda}$					0.215±0.054	
Ξ^+/Ξ^-					0.853±0.1	
Ξ^-				†2.05±0.2		
Ξ^+				†1.3±1		
Ω/h^-					0.0012±0.0005	
$(\Omega + \bar{\Omega})/h^-$					0.0022±0.0007	
$\bar{\Omega}/\Omega$					0.95±0.01	
K_S/K^-						0.23±0.05
$K(892)0/K^-$					0.26±0.08	
$V, dV/dy$ [fm ³]	4569±497	5462±476	6293±1051	1500*	1127±655	956±196
T [MeV]	140*	140*	139.3±0.004	140*	140±14	140±1
λ_q	1.38±0.04	1.30±0.03	1.27±0.04	1.13±0.03	1.077±0.046	1.063±0.081
λ_s	1.127*	1.097*	1.090*	1.051*	1.017*	1.021*
γ_q	1.64*	1.64*	1.64*	1.64*	1.64±0.1	1.64±0.3
γ_s	1.80*	2.20*	2.26±0.40	1.64*	2.21±0.6	2.48±0.5
λ_{I3}	0.983±0.003	0.986±0.002	0.988±0.002	0.994±0.002	0.994±0.008	0.997±0.004
μ_B [MeV]	134	109	98	50.6	31.3	25.7
μ_S [MeV]	28.0	23.2	20.7	10	7.97	5.60

sistency test of SHM allowing a prediction to be made of other $N_{4\pi}$ we show in table IV. This consideration is also yielding a rapidity-averaged value of T and of the 5 chemical parameters, as well as an estimate of the proper size V of the hadronizing fireball.

The value of μ_B , which varies as function of rapidity to follow the highly variable baryon distribution [44], is found at a median value, seen at the bottom of table III, on left for the $N_{4\pi}$ fits. We consider it to be experimentally motivated hadron yield prediction. For this reason, we do not discuss the fit quality of $N_{4\pi}$ yields at RHIC but we discuss the expected total particle yields.

We extend the consideration of the $N_{4\pi}$ yields to the lower energies, $\sqrt{s_{NN}} = 62.4$ and 130 GeV. This can be

done assuming that there is no change in physics between top SPS energy and RHIC 200 GeV run. Thus, the success of our particle yield prediction would be a confirmation of this hypothesis. Our procedure can be seen in detail on the left of table III. We fix the hadronization temperature at $T = 140$ MeV, choose the value $\gamma_q \simeq e^{m_\pi/2T}$, and interpolate the values of γ_s . We do find the required values of λ_q , λ_{I3} and V needed to assure the total baryon yield, fraction of charge Q/b and one particle yield, which we choose to be π^+ . We use the observation that the π^+ yield from Brahms connects in a logarithmic plot in a nearly perfect straight line with the SPS energy domain. This produces the π^+ interpolated values we introduced in table III. The fit succeeds perfectly and allows us to

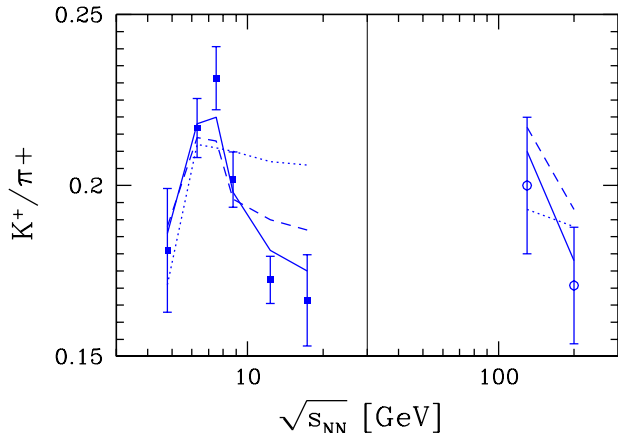


FIG. 2: K^+/π^+ yields (filled squares) as function of $\sqrt{s_{NN}}$, at RHIC the ratio applies to central rapidity. The solid lines show our model fit. The chemical equilibrium fit result is shown by the dotted line. The dashed line arises finding best γ_s for $\gamma_q = 1$.

offer predictions for the total particle yields presented in table IV.

We present, in detail, the resulting particle multiplicities in table IV for RHIC. On left, we show the expected total yields and on right the central rapidity yields. We recall that among total yields only at 200 GeV a significant experimental input was available, thus the 62.4 and 130 GeV total yield results are an educated guess satisfying all constraints and criteria of the SHM model. Similarly, the central rapidity region yields for 62.4 GeV is a prediction based on interpolated yields, with inputs seen in table III. All results presented are obtained with the following weak decay set of assumptions. All Σ^\pm (and antiparticle) weak decay products are always accepted, as are the K_S decay products due to their short lifespan. 10% of K_L decay products are accepted. For the presented predictions, we accept all baryons arising from decays of the hyperons, and at 130 GeV also the mesons from hyperon decays.

D. Energy dependent particle yields

We consider, more systematically, the energy dependence of particle yields and ratios. Of particular interest is the ratio K^+/π^+ which shows the previously unexplained horn structure. We compare the experimental and theoretical behavior in figure 2. We recall that the abrupt increase in the value of γ_q occurs near to where the rise in K^+/π^+ changes slope and begins to decrease with reaction energy. The solid line, shows our fit which reproduces the horn structure well. The (central rapidity) RHIC portion is separated on right in figure 1. The AGS and SPS results are on left.

The dotted line, in figure 2, presents best fit results

TABLE IV: Output hadron multiplicity data obtained in this work for RHIC energy range. See text for the meaning of predictions of $N_{4\pi}$ yields at 62.4 and 130 GeV and of dN/dy at 62.4 GeV. The input statistical parameters are seen in table III. $b = B - \bar{B} \equiv N_W$ for 4π results and $b = d(B - \bar{B})/dN$ for results at central rapidity. Additional significant digits are presented for purposes of tests and verification.

$\sqrt{s_{NN}}$ [GeV]	62.4	130	200	62.4	130	200
E_{eq} [GeV]	2075	9008	21321	2075	9008	21321
Δy	± 4.2	± 4.93	± 5.36	± 4.2	± 4.93	± 5.36
	$N_{4\pi}$ 5%			$dN/dy _{y=0}$ 5%		
b	350.2	350.2	350.1	37.77	18.96	15.0
π^+	1140	1450	1641	362.4	300.5	276.3
π^-	1233	1555	1748	372.4	307.2	281.2
K^+	185.5	266.9	301.8	48.8	50.2	49.3
K^-	131.4	201.2	234.2	43.2	45.5	46.0
K_S	212.3	225.7	258.3	44.6	46.0	45.7
ϕ	17.4	31.1	36.1	4.74	6.48	7.22
p	212.3	237.0	248.8	39.11	30.13	28.10
\bar{p}	38.5	61.8	73.3	20.31	20.70	20.58
Λ	89.3	121.4	131.2	16.9	16.9	17.5
$\bar{\Lambda}$	22.4	40.8	48.5	9.88	12.6	13.6
Ξ^-	10.7	17.0	18.9	2.06	2.55	2.87
Ξ^+	3.48	7.01	8.35	1.33	2.04	2.33
Ω	1.07	2.17	2.48	0.21	0.36	0.47
$\bar{\Omega}$	0.52	1.24	1.48	0.16	0.33	0.41
$K^0(892)$	37.9	55.2	62.5	11.15	11.3	11.2
Δ^0	27.9	27.8	28.5	5.03	3.31	2.84
Δ^{++}	27.0	27.1	27.8	4.98	3.27	2.82
$\Lambda(1520)$	4.33	5.47	5.79	0.81	0.73	0.72
$\Sigma^+(1385)$	8.23	10.42	11.12	1.56	1.40	1.38
$\Xi^0(1530)$	2.86	4.58	5.06	0.56	0.69	0.78
η	102.6	136.3	154.5	32.0	28.1	26.3
η'	7.66	10.43	11.75	2.38	2.17	2.06
ρ^0	83	100	111	26.2	20.1	17.8
$\omega(782)$	71.9	86.8	96.6	23.6	18.0	15.9
$f_0(980)$	6.69	9.78	11.11	2.01	2.03	2.01
$\Theta^+(1540)$	6.46	7.62	7.85	0.94	0.82	0.79
$(s - \bar{s})/(s + \bar{s})$	0	0	0	0	0	0

obtained within the chemical equilibrium model, i.e., with $\gamma_s = \gamma_q = 1$, using the same computer program (SHARE), and the same data set. We see that the chemical equilibrium SHM cannot explain the horn in the K^+/π^+ ratio. The dashed line corresponds to the result obtained fixing $\gamma_q = 1$ but allowing γ_s to assume a best value. We see that, without $\gamma_q > 1$, it is difficult if not impossible to obtain the large reduction of K^+/π^+ ratio with increasing energy.

A graphic comparison of the experimental input and theoretical output particle yields as function of energy for several other particles is seen in figure 3. We show K^-/π^- with Λ/π^+ , Xi^-/π^- with $5 \times \Omega^-/\pi^-$, $\Xi^+/\bar{\Lambda}$ with $2\bar{\Omega}/\Xi^+$ and at bottom $\phi/\sqrt{\pi^+\pi^-}$. We are showing the total SHM yields at AGS/SPS and RHIC, connected by a solid line. The central rapidity yields are denoted (in red) by the dashed lines. Circles denote values used in fit which are due to interpolation and are not result of

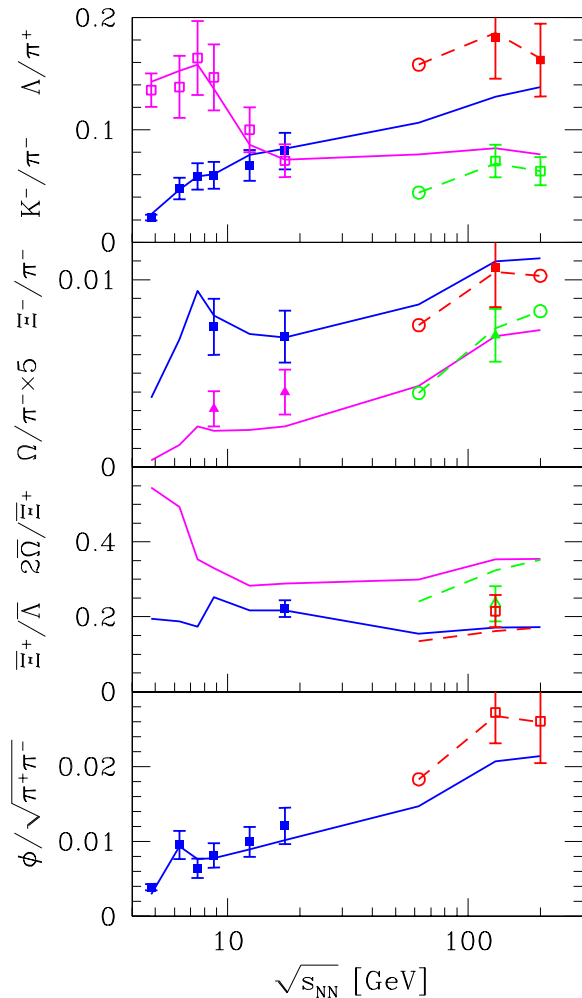


FIG. 3: Comparison of experimental and theoretical ratios of particle yields as function of reaction energy $\sqrt{s_{\text{NN}}}$ — theoretical SHM total $N_{4\pi}$ results are connected by solid lines. The dashed lines connect the central rapidity dN/dy results at RHIC. Experimental data input is shown with error bar. The open circles without error are yields obtained by interpolation in energy of experimental results.

experimental measurement.

The SHM with chemical non-equilibrium reproduces practically all features of the experimental particle yield data well as function of energy. We already discussed the K^+/π^+ ratio in figure 2. In figure 3, we note in the top panel the well described shift of s quark population from its dominant baryon, to meson carriers. There is an interesting horn predicted in the multi-strange baryon Ξ^-/π^- yield. We underpredict by 1–1.5s.d. the yields of Ω , for both SPS results, as function of energy. Excess of Ω may be due to a non SHM source of these particles, such as chiral condensate [45].

Of particular importance, in the study of quark–gluon plasma formation, is strange antibaryon enhancement.

It is one of important signatures of deconfinement [47]. These particles are hard to make in conventional environment, and also are highly sensitive probes of the medium from which they emerge. There is still precious little data available for the antibaryon ratios of interests, $\Xi^-/\bar{\Lambda}$ and $2\bar{\Omega}/\Xi^+$, we see one entry for SPS and one entry at central rapidity for RHIC in figure 3. Due to the nature of strange antibaryons as sensitive probes of the medium as we argue in the next paragraph, what we see is, in essence, a completely flat curve, with minor fluctuations originating in the other experimental data and amplified by the sensitivity of these particles. Another important point is that these ratios are relatively large, and hard to understand other than quark chemistry picture. It would be very interesting to see if at AGS energy scale $2\bar{\Omega}/\Xi^+$ is indeed that large which would establish quark chemistry in this environment.

The strange antibaryon enhancement phenomenon has been, however, studied in depth comparing yields of antibaryons to a baseline yield obtained scaling the pp or pBe yields, considering the effect as function of impact parameter and reaction energy [46]. In this work, we can, for the first time, study the energy dependent rise in the yields of $\bar{\Lambda}$, Ξ^+ and $\bar{\Omega}^+$. At this time, only the $\bar{\Lambda}$ production is experimentally available. All three rates, shown in figure 4, are predicted to rise at nearly the same rate as function of $\sqrt{s_{\text{NN}}}$ — indeed the strange antibaryon ratios we have shown in figure 3 are as good as flat compared to the great variability of the absolute yields rising very rapidly as is seen in figure 4. Once the deconfined phase is formed, the ratios of yields of strange antibaryons should not change. What we see is that, in the entire energy range we explored, these ratios are in fact constant. This maybe taken as an indication that the transition we observe at $\sqrt{s_{\text{NN}}^{\text{CT}}}$ involves deconfined phases of different structure. We will further discuss this in section IV.

III. FIREBALL PROPERTIES AT BREAKUP

A. Energy dependence of model parameters

The statistical parameters of the SHM are shown, as function of $\sqrt{s_{\text{NN}}}$, in figure 5, for the entire energy domain. From top to bottom, we see the chemical freeze-out temperature T , the statistical occupancy parameters γ_q and γ_s/γ_q and the chemical potentials μ_B and μ_S . The error bars comprise the propagation of the experimental yield errors, as well as any uncertainty due to the shape of the $\chi^2/\text{d.o.f.}$ minimum, seen in figure 1. The (red) triangle results are for the RHIC dN/dy case, while (blue) squares are for the $N_{4\pi}$ data throughout the energy domain and include the estimates we made for the RHIC energy range (at $\sqrt{s_{\text{NN}}} = 62.4$ and 130 GeV we show for these no fit error as this is solely our estimate).

The only significant difference between RHIC dN/dy and $N_{4\pi}$ results is noted for the chemical potentials μ_B

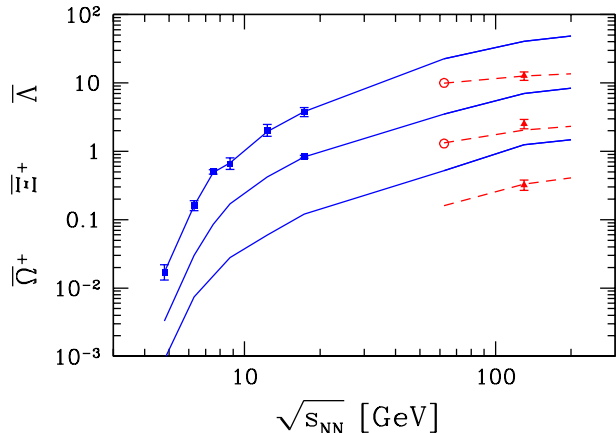


FIG. 4: Yields of strange antibaryons as function $\sqrt{s_{NN}}$, from top to bottom $\bar{\Lambda}$, $\bar{\Xi}^+$ and $\bar{\Omega}^+$. The solid lines connect the results of SHM $N_{4\pi}$ fit to particle data. The AGS/SPS energy range $N_{4\pi}$ yields (in blue) on left and RHIC $N_{4\pi}$ on right. Also on right (in red, connected with dashed lines) are the central dN/dy yields. The yields at $\sqrt{s_{NN}} = 62.4$ used in our study are result of interpolation of RHIC and SPS results.

and μ_S and shown in the bottom panel (note logarithmic scale). The baryochemical potential μ_B drops relatively smoothly as the reaction energy is increased. The vertical line indicates the observed sudden change in the structure of the fireball. This is seen in all statistical variables, but most clearly in γ_q .

It is important to recall that we present γ_i evaluated using hadronic multiplicities. If these arise from breakup of a quark fireball, the quark-side occupancy parameters could be considerably different. The hadron side phase space size is in general different from the quark-side phase space, since the particle degeneracies, and masses, are quite different. In the study of the breakup of the quark fireball into hadrons, we can compute the resultant hadron phase space occupancy for two extreme limits.

First, consider a fast transformation (sudden breakup) of the quark phase. This occurs nearly at fixed volume. To accommodate the difference in the momentum part of the phase space, the chemical occupancy non-equilibrium parameters γ_i undergo an abrupt change. We note that it is of no importance if there was or not a phase transition between the phases, what matters is that there was no time to reequilibrate chemically the quark yields. In the opposite limit of a very slow transformation of phases, there is available a prolonged period in time in which the volume of the system can change to accommodate the appropriate number of particles in chemical equilibrium corresponding to the maximum entropy content.

To determine the change in γ_i in sudden hadronization, one needs to compare in detail the phase space of quark phase with that of hadron gas. For $\mu_B = 0$, as well as small chemical potentials $\mu_B/T < 1$, lattice evaluation of the deconfined phase properties are available [50, 51].

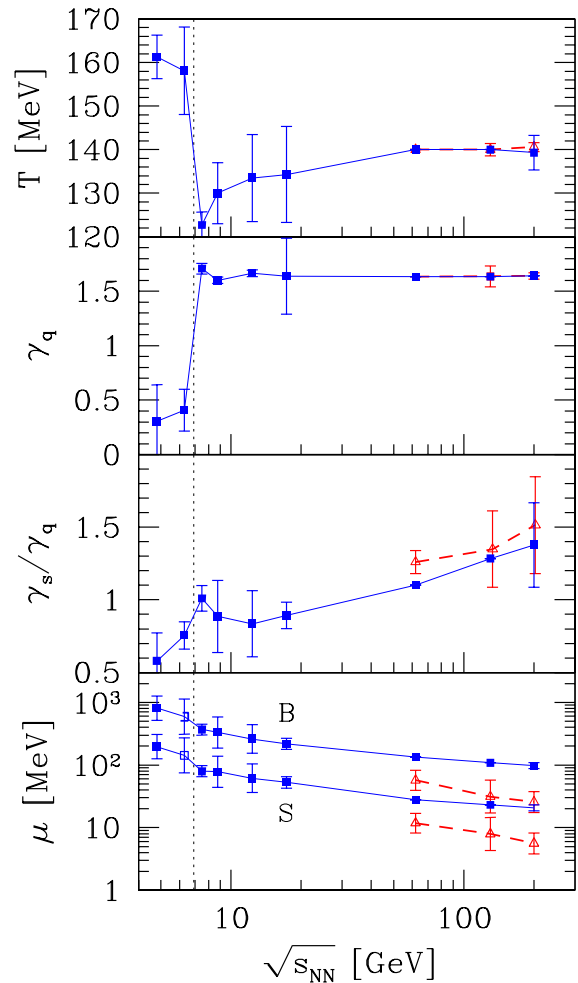


FIG. 5: Statistical parameter results for $N_{4\pi}$ (blue online, square). From top to bottom: T , γ_q , γ_s/γ_q and μ_B, μ_S [MeV], as function of $\sqrt{s_{NN}}$. The lines guide the eye. Same for dN/dy at RHIC (red online triangles).

It is thus possible to model quantitatively the properties of the deconfined phase. For $\mu_B = 0$, the occupancy on hadron side is found to be greater by a factor two than on the quark side [52]. Thus, the large values of γ_s^{HG} and γ_q^{HG} seen in figure 5 at large $\sqrt{s_{NN}}$ could be consistent with sudden breakup of chemically equilibrated primordial QGP phase. Other dynamic effects, in particular fast expansion, in general also favor an over-saturated phase space with $\gamma_i > 1$.

As seen in figure 5, γ_s/γ_q rises at first rapidly, as expected if strangeness production is delayed by a greater threshold mass and has to catch up with the light hadron production. γ_s/γ_q decreases beyond the edge of energy threshold, as can be expected due to the conversion of the quark to hadron occupancy discussed above. The rise resumes and continues for all energies above 80 AGeV (note that, at RHIC only, results showing an error can be considered to arise from a fit).

TABLE V: The physical properties: Pressure P , energy density $\epsilon = E_{\text{th}}/V$, entropy density S/V , strangeness density s/V for AGS and CERN energy range (top line projectile energy E [GeV]). Bottom: dimensionless ratios of properties as fireball breakup, P/ϵ and E_{th}/TS .

$E[\text{AGeV}]$	11.6	20	30	40	80	158
$\sqrt{s_{\text{NN}}} [\text{GeV}]$	4.84	6.26	7.61	8.76	12.32	17.27
$P[\text{MeV}/\text{fm}^3]$	23.8	18.9	56.7	62.7	68.2	66.1
$\epsilon[\text{MeV}/\text{fm}^3]$	206.1	146.7	411.7	437.9	443.1	411.6
$S/V[1/\text{fm}^3]$	1.42	1.05	4.05	4.07	4.155	3.91
$100\bar{s}/V[1/\text{fm}^3]$	1.07	1.43	5.45	6.32	6.74	6.44
$\rho_b[1/\text{fm}^3]$	0.113	0.0648	0.176	0.167	0.131	0.0984
P/ϵ	0.115	0.129	0.138	0.143	0.154	0.161
E_{th}/TS	0.90	0.88	0.83	0.83	0.80	0.785

B. Physical properties

We now turn our attention to the physical properties of the hadronizing fireball obtained summing individual properties of hadronic particles produced, both those observed experimentally, and those predicted in terms of SHM fit to the available results. We include, in this consideration, the average properties of the RHIC energy systems obtained from particle yields which, except at the top energy $\sqrt{s_{\text{NN}}} = 200$ GeV, are mostly result of interpolation of particle yields and/or an educated guess about the statistical SHM parameters. One can see the consideration of the physical properties of the fireball at breakup as another way to present the SHM parameters. For example, the net baryon density, $\rho_b \equiv (B - \bar{B})/V$, is most directly related to the baryochemical potential μ_B .

We present the physical properties, i.e., pressure P , energy density ϵ , entropy density S/V , net baryon density $\rho_b \equiv (B - \bar{B})/V$ and the yield of strangeness s , in table V for the AGS/SPS energy range considered. Note that s contains hidden strangeness from η, ϕ, η' . At the bottom of table V, we show the dimensionless ratios of extensive variables P/ϵ , and E/TS . These two ratios are very smooth as function of energy, and lack any large fluctuations that could be associated with fit error. These ratios are characteristic for the conditions of the fireball at the point of hadronization. The values presented must be understood in terms of future dynamical models of the fireball breakup process. We present the energy range at RHIC on left in table VI. We recall that the 62.4 GeV and the 130 GeV 4π results, as well as in part the 200 4π results, are result of considerations which do not involve experimental measured particle yields. Thus, the 4π results are to be seen as SHM sophisticated prediction. On right, in table VI, we present the results for central rapidity densities. Here, only the 62.4 GeV case is a prediction, the other results are direct consequence of the data interpretation in terms of SHM.

The fit uncertainty in the quantities presented in tables V and VI is difficult to evaluate in detail. The individual physical properties require powers and exponents

TABLE VI: The physical properties for RHIC energy range, see table V for details. All 62.4 GeV results and the 130 GeV 4π results as well as in part the 200 4π results are, as discussed in text, a prediction. For the central rapidity case, we show the rapidity densities: energy rapidity density $d\epsilon = dE_{\text{th}}/dV$, entropy rapidity density dS/dV , strangeness rapidity density ds/dV and net baryon rapidity density db/dV .

$\sqrt{s_{\text{NN}}} [\text{GeV}]$	62.4	130	200	62.4	130	200
	$N_{4\pi}$			$dN/dy _{y=0}$		
$P[\text{MeV}/\text{fm}^3]$	83.9	88.3	86.0	77.7	85.6	92.2
$dE_{\text{th}}/dV[\text{MeV}/\text{fm}^3]$	514.5	544.5	527.2	455.6	515.6	564.0
$dS/dV[1/\text{fm}^3]$	4.72	4.98	4.86	4.26	4.76	5.16
$100d\bar{s}/dV[1/\text{fm}^3]$	9.50	11.7	11.5	8.10	11.3	13.4
$100db/dV[1/\text{fm}^3]$	7.66	6.41	5.56	2.52	1.68	1.56
PdV/dE_{th}	0.163	0.162	0.163	0.170	0.166	0.163
dE_{th}/TdS	0.78	0.78	0.78	0.76	0.77	0.78

of statistical parameters, and thus, at first, we expect that the fractional errors are increased, as compared to those prevailing among statistical parameters in table I. However, the dominant contributions to each physical property could be directly derived from the individual observed particle yields and a large compensation of errors originating in the fitted statistical parameter errors must occur.

For example, most of the pressure at breakup is due to the most mobile, lightest particle, the pion. These yields are known to better than 10%, and thus, the pressure must be known to greater precision since there are further constraints from consistency of this yield with the yield of other particles. It is for this reason that the results when presented graphically (see figure 6) are at 5% level smooth functions of $\sqrt{s_{\text{NN}}}$, with fluctuations apparently at worse similar to those we see in the individual statistical SHM parameters. In future, one could hope to fit to the experimental data directly the physical properties, bypassing the statistical parameters. This can be done, in principle, considering the mathematical properties of these expressions. However, such study transcends considerably the scope of this paper, and it is indeed motivated by results we present for the first time here.

On the left hand side, in figure 6, we see from top to bottom the baryon density, the thermal energy density ϵ and the entropy density σ . On the right hand side, from top to bottom, we show the pressure P , and the dimensionless ratio of pressure to thermal energy density P/ϵ , and $E/TS = \epsilon/T\sigma$. The triangles (red) correspond to the properties of the fireball at central rapidity. We note the significant difference for the total fireball averages (squares) and the central rapidity result in the net baryon number density at RHIC energy scale.

As the reaction energy passes the threshold, $6.26 \text{ GeV} < \sqrt{s_{\text{NN}}^{\text{CT}}} < 7.61 \text{ GeV}$, the hadronizing fireball becomes much denser: the entropy density jumps by factor 4, and the energy and baryon number density by a factor 2-3. The hadron pressure increases from

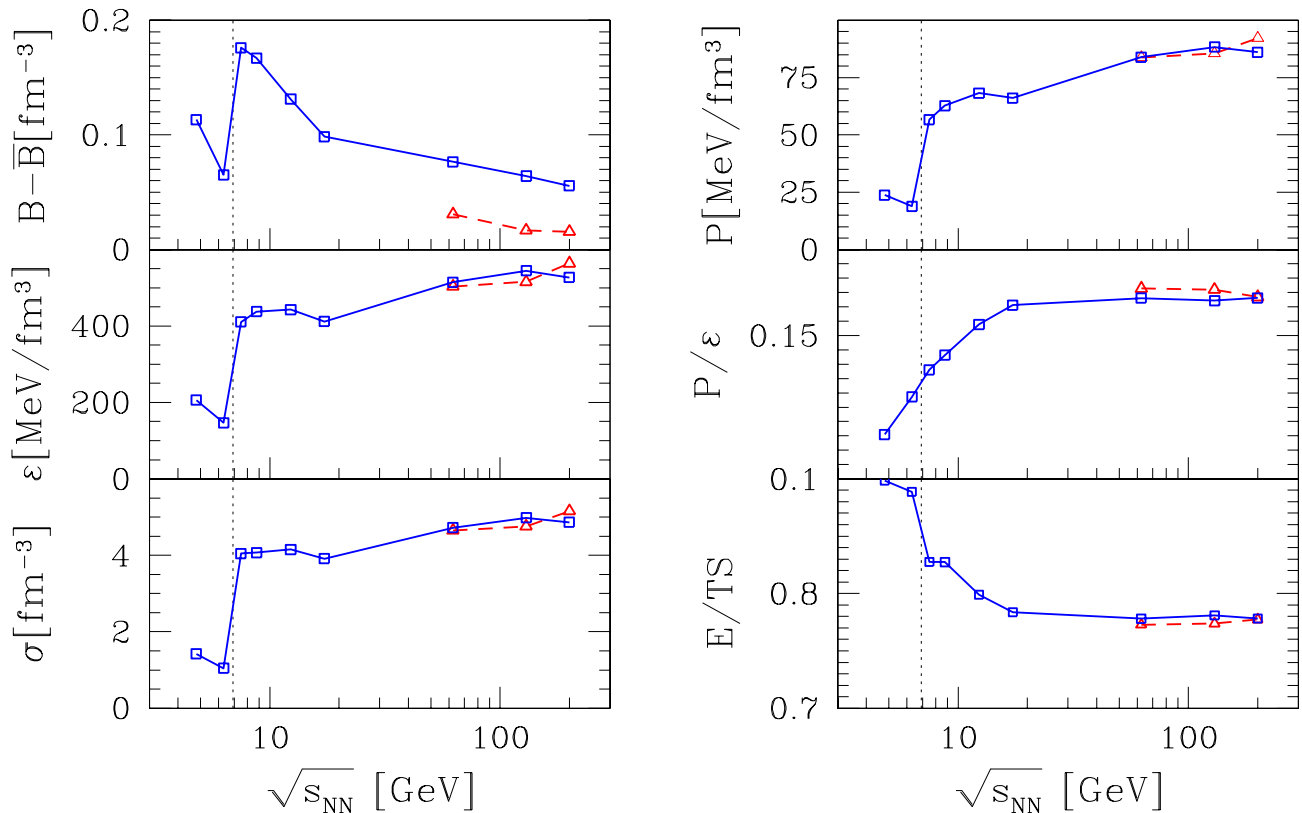


FIG. 6: From top to bottom, on left hand side the baryon density $B - \bar{B}[\text{fm}^{-3}]$, energy density $\epsilon[\text{MeV}/\text{fm}^3]$, and entropy density $\sigma[\text{fm}^{-3}]$, as function of $\sqrt{s_{\text{NN}}}$, on right hand side pressure $P[\text{MeV}/\text{fm}^3]$, P/ϵ , and $E/Ts = \epsilon/T\sigma$. Squares(blue) average over the entire fireball at hadron freeze-out, triangles (red) for the central rapidity region of the fireball.

$P = 25 \text{ MeV}/\text{fm}^3$ initially by factor 2, and ultimately more than factor 3. There is a more gradual increase of $P/\epsilon = 0.115$ at low reaction energy to 0.165 at the top available energy. Also E/Ts falls gradually from 0.9 down to 0.78 for the high density fireball. The rather rapid change in the individual properties: entropy, energy, pressure is seen, in figure 6, to be largely compensatory, resulting in a smooth change in P/ϵ , and similarly E/Ts . Even though there is a small reminder of the sudden changes in its three factors in the ratio E/Ts , this quantity is extraordinarily smooth. Any structure model of the phase transformation and the two phase structure will need to address these chemical freeze-out condition results quantitatively.

These two ratios E/Ts and P/ϵ are related. Restating the 1st law of thermodynamics:

$$\frac{E}{TS}(1+k) = 1 + \frac{\sum_i \nu_i \ln \Upsilon_i}{\sigma}, \quad k = \frac{P}{\epsilon}. \quad (6)$$

For each hadron fraction with density ν_i the total fugacity is

$$\Upsilon_i = \prod_j \gamma_j^{n_j} \lambda_j^{n_j}, \quad (7)$$

where all valance quarks and antiquarks of each hadron fraction contribute in the product, see section 2 in [13]. In the limit of chemical equilibrium:

$$\frac{\sum_i \nu_i \ln \Upsilon_i}{\sigma} \rightarrow \frac{(B - \bar{B})\mu_B}{T\sigma}. \quad (8)$$

Thus in this limit at the RHIC energy range, we expect that $E/Ts \rightarrow 1/(1+P/\epsilon)$. However, the results in figure 6 show, the chemical non-equilibrium effects contribute considerably.

It is interesting to note that exactly the same behavior of the physical properties of the fireball has also been obtained as function of the volume in the study of impact parameter dependence, see figure 4 in [3]. In fact, the results we derived here show an unexpected universality of the hadronizing fireball, which depends solely on the question if it occurs ‘below’ or ‘above’ the threshold in energy and volume size; the volume threshold corresponds to critical participant number $13.4 < A^{\text{cf}} < 25.7$.

C. Strangeness and Entropy yield

The yield of strangeness produced, should the deconfined QGP fireball be formed, is sensitive to the initial

conditions, especially temperature achieved. The standard results for strangeness relaxation time corresponds to $\tau_s(T = 300 \text{ MeV}) \simeq 2 \text{ fm}/c$ [48]. When this result is used in model calculations addressing RHIC [49], one finds, assuming gluon thermal and chemical equilibrium, that the thermal strangeness production in the early stage suffices to saturate the QGP fireball phase space at hadronization.

Even so, there is considerable uncertainty how short the time required to relax strangeness flavor is, as the relaxation time lengthens with the square of the glue phase space under-occupancy, $\tau_s \propto 1/\gamma_G^2$. Much of the uncertainty about the gluon chemical conditions prevailing in the initial thermal phase can be eliminated by considering the ratio of the number of strange quark pairs to the entropy s/S . In the QGP, the dominant entropy production occurs during the initial glue thermalization $\gamma_G \rightarrow 1$, and the thermal strangeness production occurs in parallel and/or just a short time later. Moreover, both strangeness s and entropy S are nearly conserved in hadronization, and thus, the final state yield value for the ratio s/S is directly related to the kinetic processes in the fireball at $\tau \simeq 1\text{--}3 \text{ fm}/c$.

We first estimate the magnitude of s/S in the QGP phase considering, in the hot early stage of the reaction, an equilibrated non-interacting QGP phase with perturbative properties:

$$\begin{aligned} \frac{s}{S} \equiv \frac{\rho_s}{\sigma} &= \frac{\gamma_s^{\text{QGP}}(3/\pi^2)T^3(m_s/T)^2 K_2(m_s/T)}{(32\pi^2/45)T^3 + n_f[(7\pi^2/15)T^3 + \mu_q^2 T]}, \\ &= \frac{0.027\gamma_s^{\text{QGP}}}{1 + 0.054(\ln \lambda_q)^2}. \end{aligned} \quad (9)$$

Here, we used for the number of flavors $n_f = 2.5$ and $m_s/T = 1$. We see that the result is a slowly changing function of λ_q , for large $\lambda_q \simeq 4$ we find at lowest SPS energies, the value of s/S is reduced by 10%. Considering the slow dependence on $x = m_s/T \simeq 1$ of $W(x) = x^2 K_2(x)$, there is further dependence on the temperature T .

The rise with reaction energy toward the limiting value, $s/S = 0.027$ for large $\sqrt{s_{\text{NN}}}$, is driven by the decrease in $\lambda_q \rightarrow 1$ and, importantly, by an increase in chemical strangeness equilibration with the QGP occupancy $\gamma_s^{\text{QGP}} \rightarrow 1$. The dependence on the degree of chemical equilibration which dominates the functional behavior with $\sqrt{s_{\text{NN}}}$ is:

$$\frac{s}{S} = \frac{0.027\gamma_s^{\text{QGP}}}{0.38\gamma_G + 0.12\gamma_s^{\text{QGP}} + 0.5\gamma_q^{\text{QGP}} + 0.054\gamma_q^{\text{QGP}}(\ln \lambda_q)^2}. \quad (10)$$

Thus, we expect to see

Eq.(10) predicts a smooth increase in s/S toward its maximum value which by counting the degrees of freedom appears to be $s/S \rightarrow 0.027$, while the QGP source of particles approaches chemical equilibrium with increasing collision energy and/or increasing volume. It is important to keep in mind that the ratio s/S is established

TABLE VII: AGS and CERN energy range (see top lines for projectile energy E [GeV] and $\sqrt{s_{\text{NN}}}$): Strangeness yield s ($= \bar{s}$), strangeness per entropy s/S , strangeness per baryon s/b , the energy cost to make strangeness pair $\sqrt{s_{\text{NN}}}/(2s/b)$, thermal energy per baryon at hadronization E_{th}/b , fraction of initial collision energy in thermal degrees of freedom, $(2E_{\text{th}}/b)/\sqrt{s_{\text{NN}}}$.

E [AGeV]	11.6	20	30	40	80	158
$\sqrt{s_{\text{NN}}}$ [GeV]	4.84	6.26	7.61	8.76	12.32	17.27
b	383.2	348.5	349.5	349.6	349.8	361.9
\bar{s}	36	76.9	108	132	179.5	237
$100\bar{s}/S$	0.75	1.4	1.3	1.55	1.63	1.65
\bar{s}/b	0.094	0.22	0.31	0.38	0.51	0.65
$\sqrt{s_{\text{NN}}}/(2\bar{s}/b)$ [GeV]	26.1	14.2	12.3	11.6	12.1	13.2
E_{th}/b [GeV]	1.82	2.26	2.34	2.62	3.38	4.18
$(2E_{\text{th}}/b)/\sqrt{s_{\text{NN}}}$	0.754	0.723	0.615	0.598	0.548	0.484
E_{th}/\bar{s} [GeV]	19.4	10	7.55	6.9	6.6	6.4

TABLE VIII: Top section: SHM yields of baryon b and at central rapidity db/dy , and strangeness s and ds/dy at RHIC, left for the total system, right for the central rapidity region. The 62.4 GeV results and the 130 GeV 4π results as well as in part the 200 4π results are, as discussed in text, a prediction. Next, we give (left for full reaction volume, right for the central rapidity domain) strangeness per entropy s/S (for central rapidity ds/dS , strangeness per baryon s/b), the energy cost to make strangeness pair $\sqrt{s_{\text{NN}}}/(2ds/db)$, thermal energy per baryon at hadronization dE/db , fraction of initial collision energy in thermal degrees of freedom, $(2E_{\text{th}}/b)/\sqrt{s_{\text{NN}}}$. The differential notation allows to cover both cases, total and central rapidity yields.

$\sqrt{s_{\text{NN}}}$ [GeV]	62.4	130	200	62.4	130	200
	$N_{4\pi}$			$dN/dy _{y=0}$		
$b, db/dy$	350	350	350	37.8	18.9	14.9
$\bar{s}, d\bar{s}/dy$	434	639	724	121.5	127	128
$100\bar{s}/S, d\bar{s}/dS$	2.0	2.35	2.37	1.90	2.37	2.60
$\bar{s}/b, d\bar{s}/db$	1.24	1.82	2.07	3.21	6.73	8.59
$\sqrt{s_{\text{NN}}}/(2d\bar{s}/db)$ [GeV]	25.2	35.7	48.3	9.71	9.66	11.64
dE_{th}/db [GeV]	6.72	8.49	9.48	18.0	30.7	36.2
$(2dE_{\text{th}}/db)/\sqrt{s_{\text{NN}}}$	0.215	0.131	0.095	0.577	0.472	0.362
$dE_{\text{th}}/d\bar{s}$ [GeV]	5.42	4.65	4.58	5.62	4.56	4.21

early on in the reaction, and the above relations and associated chemical conditions we considered apply to the early hot phase of the fireball. At hadron freeze-out, the QGP picture used above does not apply. Gluons are likely to freeze faster than quarks and both are subject to much more complex non-perturbative behavior. However, both strangeness and entropy, once created, cannot disappear as the more complex low temperature domain is developing.

In tables VII and VIII, we present, in top portion, the strangeness production as function of reaction energy at AGS/SPS and RHIC, respectively. We give the baryon content and the total strangeness content of the fireball derived from the SHM fit to particle yield. Below, we see the above discussed strangeness per entropy s/S re-

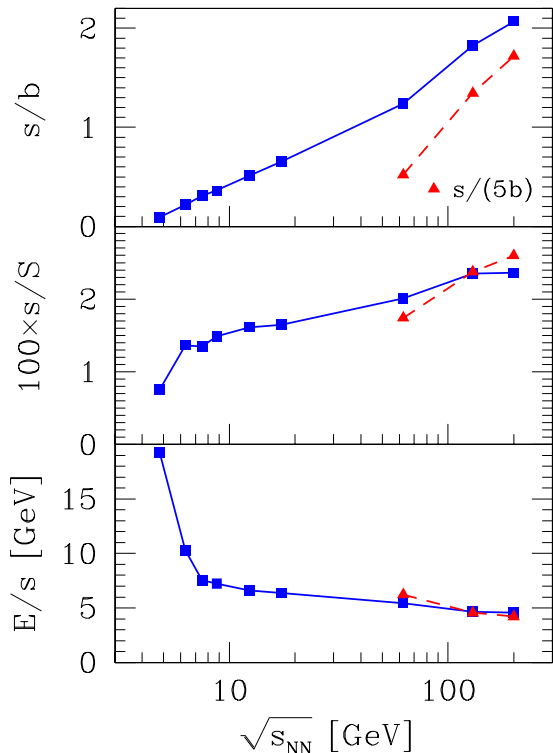


FIG. 7: The specific strangeness yield as function of reaction energy $\sqrt{s_{\text{NN}}}$. Top strangeness per baryon s/b , middle strangeness per entropy s/S and bottom thermal energy content per strangeness. Solid squares correspond to $N_{4\pi}$ the triangles on right are for the rapidity density yield dN/dy at RHIC. The total yield results are connected by solid line to guide the eye, and the central rapidity results (red) are connected by dashed line.

tio, and strangeness per net baryon number s/b ratio. We present the increasing specific strangeness per baryon and per entropy yields in figure 7, two top panels. The remarkable result we find is that the specific per entropy yield of strangeness converges for top RHIC energy and central rapidity toward the QGP result obtained counting the degrees of freedom, see Eq. (9). The somewhat smaller values for the 4π case are consistent with the average being made over the fragmentation region. This effect is greater in the ratio s/b as we have to count all participant baryons.

The middle section, in table I, shows the center of momentum energy cost $\sqrt{s_{\text{NN}}}/(2s/b)$ to make one strangeness pair. The microcanonical input variables, s/V and b/V , for this entry vary significantly along with, and as function of $\sqrt{s_{\text{NN}}}$. Yet, we see that the result obtained varies smoothly, at first it diminishes finding a minimum at around $E = 40$ AGeV and it rises slowly thereafter. It is clearly more energy expansive to make strangeness at AGS, nearly by factor 2. A minimum in energy cost to make strangeness is near to 30 AGeV beam energy, at the peak of K^+/π^+ horn.

The increase in cost of making strangeness can be at-

tributed to the decreasing energy fraction stopped in the reaction. The energy stopping can be estimated by evaluating the per baryon thermal energy content E_{th}/b and obtaining from this the fraction of the initial energy converted into thermal energy in the final state, $(2E_{\text{th}}/b)/\sqrt{s_{\text{NN}}}$, which fractions steadily drops from 75% at AGS to 48% at top SPS energy.

In terms of thermal energy, the cost of making strangeness pair is given in the last line of table I. After an initial very rapid drop from AGS cost at 20 GeV to 7.5 GeV near to the top of the horn, there follows a very slow and gradual decrease. We show this result graphically in the bottom panel in figure 7. This behavior clearly shows a *rapid* but smooth change-over in the underlying mechanism of strangeness production with increasing reaction energy, between 11.6 and 30 AGeV. Once the new mechanism is fully operational, we have essentially a flat, slowly decreasing energy cost per strangeness. The drop we observe above 30 AGeV can be thought to originate in transfer of thermal energy to the kinetic energy of collective expansion which we do not record in our analysis, and thus, it is conceivable that the cost in actual energy remains constant above $\sqrt{s_{\text{NN}}^{\text{CF}}}$.

As the bottom right of table VIII indicates, the fraction of energy stopped in the central rapidity region at RHIC, $(2dE_{\text{th}}/db)/\sqrt{s_{\text{NN}}}$ is rather large, it is estimated to be 58% at $\sqrt{s_{\text{NN}}} = 62.4$ GeV decreasing to 36% at top RHIC energy. The energy cost to make strangeness remains at the SPS level, connecting smoothly to this value, for both total yield and central rapidity yield. We note, in passing, that only a small fraction, 10%, of the total energy is thermalized at the top RHIC energy considering the total fireball. 90% is evidently the energy of the collective flow, predominantly in the longitudinal direction.

The expectation of ever rising strangeness yield with $\sqrt{s_{\text{NN}}}$ are not disappointed in figure 8, but the rapid smooth rise is surprising. One finds such a result in a nearly model independent analysis adding up the \bar{s} carrier particles, which are mostly directly measured. A more precise study which adds up strangeness in the particles produced according to the SHM as seen in tables VII and VIII is shown in figure 8 – there are no-negligible contributions of unobserved hidden strangeness, in particular in the η hadron (40% $s\bar{s}$ content). We have scaled the strangeness yield to the 7% centrality with $N_{\text{W}} = 349$ for the total yields. For the central rapidity, we present results for the 5% centrality. The value at $\sqrt{s_{\text{NN}}} = 62.4$ GeV is result of fit to interpolated particle data with assumed values of certain strange hadrons and statistical parameters, see table I. We see in both figure 7 and figure 8 that we slightly underestimate the strangeness yield in this procedure.

D. Universality of volume and energy thresholds

The rather sudden changes in freeze-out parameters γ_q and T appears to be a universal behavior. We estab-

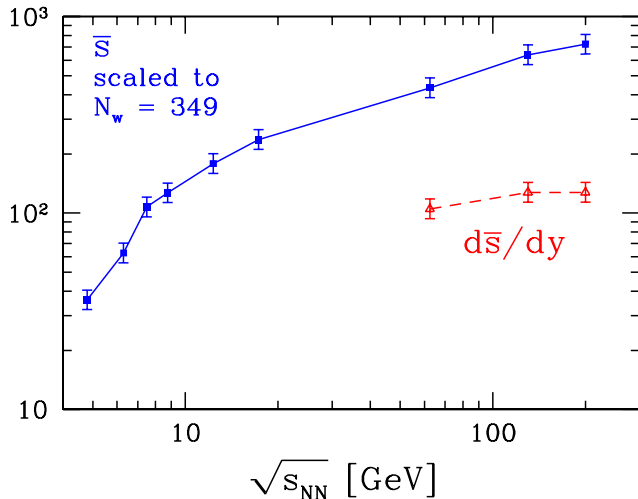


FIG. 8: The strangeness \bar{s} ($= s$) content resulting from the SHM fit, as function of reaction energy. The total yield results, solid squares (blue), are scaled with number of wounded nucleons to a fireball formed in 7% central Pb–Pb reactions ($N_w = 349$). The triangles, on right, are for the rapidity density yield $d\bar{s}/dy$ at RHIC.

lished it here as function of energy, and in earlier work as function of the reaction volume, see figure 1 in [3]. In both cases, here as function of reaction energy $\sqrt{s_{NN}}$, and earlier as function of participant number A , the chemical freeze-out temperature is higher below a threshold, as expressed either by low energy or participant number (volume size). In both cases, the most drastic change is that γ_q jumps up from a value at, or below 0.5, to 1.6 as either the energy or volume threshold is crossed. The volume threshold is, however, not as sharp as the reaction energy threshold. The large system limit is achieved for $A > 25$, with a smooth transition beginning at $A > 6$, as can be seen in figure 4 in [3].

Seeing this remark, one immediately wonders if the K^+/π^+ horn is present in the impact parameter kaon data and the answer is no. Actually, this is not surprising if we look at the horn as result of a change in physical properties involving the jump in physical properties seen in figure 6. Since $K^+/\pi^+ \propto \bar{s}/\bar{d}$, we can also understand the horn as being due to rise in density of strangeness \bar{s} followed by a rise in the \bar{d} density as function of energy, whatever the mechanism in terms of statistical parameters that implements it. However, when considering the impact parameter dependence at $\sqrt{s_{NN}} = 200$ GeV, the rise in strangeness has yet to occur, as in the small volume there was insufficient life span, and thus, we do not see the horn.

One can see the delayed production of strangeness as function of impact parameter in the PHENIX data [28], without any analysis. Consider the ratio $K/\pi \equiv \sqrt{K^+K^-/\pi^+\pi^-}$, shown in figure 9. This particular mix of particles is practically independent of chemical potentials μ_B, μ_S and the volume V as it comprises ratios of

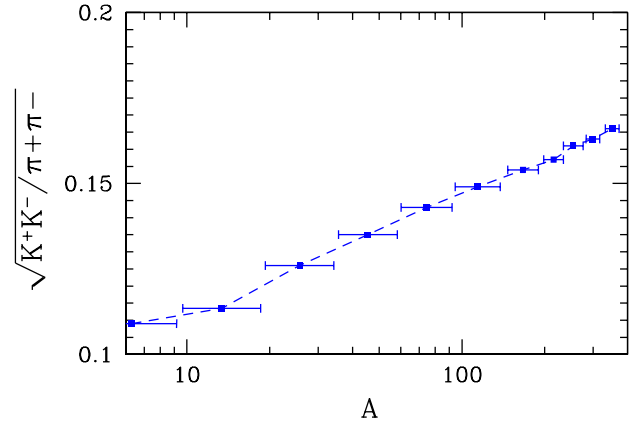


FIG. 9: $\sqrt{K^+K^-/\pi^+\pi^-}$ as function of participant number A varying with reaction centrality, PHENIX data [28].

products of particles and antiparticles. The rise seen in figure 9 is evidence for the additional strangeness production mechanism turning on at about $A \simeq 20$. Note that we do not show a common systematic error, thus the scale of the figure could undergo revision. This cannot change the insight that additional strangeness above and beyond the first collision content is produced enhancing the global yield by 50% or more. Moreover, we see that the rise is gradual as can be expected in kinetic theory models of strangeness production, and there is at the maximum centrality no sign of yield saturation.

The entropy content of the small system $A < 20$ is such that strangeness per entropy is at the level of $s/S \simeq 0.02$, and both entropy and strangeness rise with centrality of the reaction at $\sqrt{s_{NN}} = 200$ GeV. However, unlike the energy dependence, the ratio s/S rises only modestly, strangeness does not outpace entropy rise by more than 20%. This is in agreement with expectation since the threshold of strangeness mass is not fully relevant at this reaction energy, and thus we are seeing the properties of a deconfined state in which strange quark is effectively massless. There is very little if any dependence of ratios of hadron resonances with the ground state yields, such as K^*/K . This implies and agrees in quantitative way with the finding that there is no T dependence of the freeze-out conditions for $A > 20$. For this reason ratios of all hadrons which do not involve strangeness do not vary with centrality for $A > 20$.

We further note that there is little change in chemical potentials with centrality for $A > 20$, indicating that the stopping of baryons is not result of multiple scattering but is due to phase conditions of matter. Comparing other properties of matter, we see very much the same behavior as function of impact parameter and reaction energy: in particular, we note the step up in pressure, in energy density, and in entropy density at the threshold.

IV. DISCUSSION AND INTERPRETATION

A. The K^+/π^+ horn

One can wonder how, in qualitative terms, can a parameter γ_q , which controls the light quark yield, help explain the horn structure seen in figure 2. We observe that this horn structure in the K^+/π^+ ratio traces the final state valance quark ratio s/d , and in language of quark phase space occupancies γ_i and fugacities λ_i , we have:

$$\frac{K^+}{\pi^+} \rightarrow \frac{s}{d} \propto F(T) \frac{\lambda_s \gamma_s}{\lambda_d \gamma_d} \simeq F(T) \lambda_{I3} \frac{\lambda_s \gamma_s}{\lambda_q \gamma_q}. \quad (11)$$

In chemical equilibrium models $\gamma_s/\gamma_q = 1$, and the horn effect must arise solely from the variation in the ratio λ_s/λ_q and the change in temperature T . The isospin factor λ_{I3} is insignificant in this consideration. For the interesting range of freeze-out temperature, $F(T)$ is a smooth function of T . Normally, one expects that T increases with collision energy, hence we expect an monotonic increase in the K^+/π^+ ratio, not considering the quark chemistry.

As collision energy is increased, baryon transparency of colliding matter increases, yielding a decreasing $\lambda_q = e^{\mu_B/3T}$. We recall the smooth decrease of μ_B with reaction energy seen in bottom panel in figure 5. The two chemical fugacities λ_s and λ_q are coupled by the condition that the strangeness is conserved. The chemical potential effect is suggesting a smooth increase in the K^+/π^+ ratio. With considerable effort, one can arrange the chemical equilibrium fits to bend over to a flat behavior at $\sqrt{s_{NN}^{CF}}$ as the dotted line in figure 2 shows. It is quasi impossible to generate a horn with chemical equilibrium model.

Consideration of chemical non-equilibrium allows us to consider an energy dependent ratio γ_s/γ_q , which as seen in Eq.(11) is a multiplicative factor in the horn structure. The fit produces a horn like behavior of γ_s/γ_q at $\sqrt{s_{NN}^{CF}}$, seen in figure 5. As function of energy, many other particle yields must remain relatively smooth, with a few exceptions seen in figure 3. We see that the description of the horn structure is possible, as there are effectively three function of $\sqrt{s_{NN}^{CF}}$ which help to create it, T , λ_q/λ_s and γ_s/γ_q , but it is in no way assured that the right horn arises, seen the behavior with energy of the other particle yields. Indeed, only the full chemical none-equilibrium model in which the two phase space occupancies, γ_s and γ_q , vary independently, does a good job as is seen comparing the solid and dashed line in figure 2. It is thus not only the increased number of parameters, but the fact that particle production follows the SHM with chemical non-equilibrium which allows us to succeed.

B. Chemical equilibrium or non-equilibrium?

An important questions discussed in the study of hadron yields interpretations is if chemical equilibrium or non-equilibrium prevails in the hadronization process. There are workers who strongly defend chemical equilibrium [53]. Let us look again at the survey of fit quality results seen in figure 1. We note that for $\gamma_q = 1$ (but $\gamma_s \neq 1$) at each energy there seems to exist a reasonable fit with $0.5 < \chi^2/\text{d.o.f.} < 2.3$, which suggests that at each reaction energy with $\gamma_q = 1$ a reasonable and widely accepted physical description of the experimental data would emerge. This is claimed in studies that focus on the hadron yields at each energy separately. What works poorly in SHM used with $\gamma_q = 1$ and even with $\gamma_q = 1$, $\gamma_s = 1$ is the energy dependence of particle ratios, with the most prominent present day example being the horn structure in the K^+/π^+ yield ratio. Seen from this perspective it is the energy dependent particle yield that requires the inclusion in the necessary set of parameters also $\gamma_q \neq 1$.

An other important question directly related to the issue of chemical equilibrium and non-equilibrium is how the fitted results for $T(\mu_B)$, the ‘hadronization curve’ relate to the phase boundary between deconfined primary phase and the hadron phase. Clearly, the result of the fit are greatly dependent on the assumption about chemical condition with the equilibrium fit claiming a hadronization at RHIC at $T = 175$ MeV. The rapidly decreasing freeze-out temperature T as $\sqrt{s_{NN}}$ decreases, and which is certainly inconsistent with the rather flat phase transition boundary at moderate chemical potentials is explained by suggesting that the hadronization may be related to a particular values of energy per particle content, of the magnitude 1 GeV [53]. Such conditions are not rooted in any basic principles at present. The chemical equilibrium hypothesis fails to explain the hadronization conditions expected as function of T and μ_B or equivalently as function of $\sqrt{s_{NN}}$.

In summary, the interpretation of hadron production in terms of chemical equilibrium SHM disagrees, in quantitative manner, both with the reaction energy dependent particle yields (such as the K^+/π^+ horn) and the reaction energy dependent shape of hadronization boundary.

C. Hadronization boundary

We believe that the hadronization boundary, in the $T-\mu_B$ plane, is the result of a complex interplay between the dynamics of heavy ion reaction and the properties of both phases of matter, the inside of the fireball, and the hadron phase we observe. Even disregarding complications related to the rapid expansion of the dense mater fireball, the presence of chemical non-equilibrium particle distributions introduces significant freedom into the shape and location of the $T(\mu_B)$ transition region.

Recall, first, that all available lattice results apply to

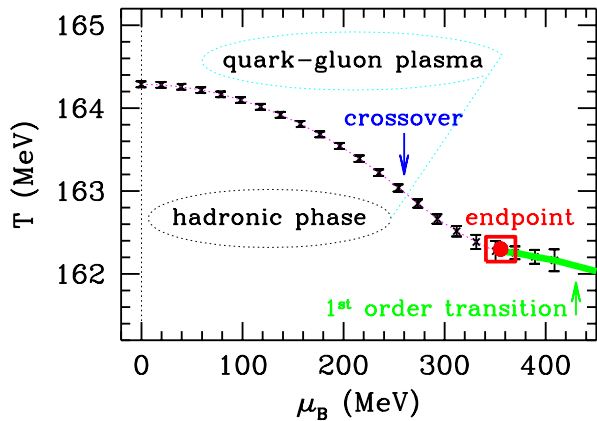


FIG. 10: Phase diagram of equilibrium hadron and quark matter, in the T - μ_B plane, for 2+1 flavors [50].

a system in the thermodynamic limit with $\gamma_q = \gamma_s = 1$. The typical boundary between the QGP and Hadron phases is shown in figure 10. A significant change in phase boundary location is to be expected when $\gamma_q, \gamma_s \neq 1$. To understand this important remark, recall the two further known cases $\gamma_q = 1, \gamma_s = 0$ corresponding to 2 flavors, and $\gamma_q = \gamma_s = 0$ corresponding to pure gauge.

Moreover, not only the location but also the *nature* of the phase boundary can be modified by variation of γ_i . We recall that for the 2+1 flavor case, there is a critical point at finite baryochemical potential with $\mu_B \simeq 350$ MeV [50]. However, for the case of 3 massless flavors there can be a 1st order transition at all μ_B [54]. This conclusion is shown in most up to date work to depend on the resulting mass of the pion [55]. Considering classical particle system, one easily sees that an over-saturated phase space, e.g., with $\gamma_q = 1.6, \gamma_s \geq \gamma_q$ for the purpose of the study of the phase transition acts as being equivalent to a system with 3.2 light quarks and 1.6 massive (strange) quarks.

Even though one should be keenly aware that over-saturation of the phase space is not the same as additional degeneracy due to true degrees of freedom, the similarity of resulting effect is great. Certainly, we can expect that for an over-saturated system there is an effective increase in the number of degrees of freedom. Looking at the structure of the quark-hadron transformation this increase in the number of available effective degrees of freedom occurs in a physical system which is almost, but not quite, able to undergo a 1st order phase transition. Therefore, we conjecture that the system with $\gamma_s > \gamma_q = 1.6$ has a true phase boundary also at small μ_B corresponding to a 1st order phase transition condition. Because of the added degrees of freedom, the phase transition temperature is at the same time decreased and thus below the cross-over value for 2+1 flavors near $T = 162 \pm 3$ MeV.

It seems to us that it would be very interesting to determine, in as more rigorous way for the case of the 2+1 flavor lattice QCD at $\mu_B = 0$ for which values, if any, of

γ_i the system undergoes a phase transition of 1st order. Lattice QCD methods employed to obtain results at finite μ_B , e.g., the power expansion [56], may be applicable to study also the case of $\mu_\gamma \equiv T \ln \gamma_i > 0$.

The dynamical, and less spectacular, effect capable to shift the location in temperature of the expected phase boundary, is due to the expansion dynamics of the fireball. The analysis of the RHIC results suggests that the collective flow occurs at parton level [57]. Collective flow of color (partons) is like a wind capable to push out the color non transparent ‘true’ vacuum [58], adding to thermal pressure the dynamical component, for a finite expanding system this would lead to supercooling [59]. This dynamical effect will push the hadronization condition to lower local freeze-out T at high $\sqrt{s_{NN}}$, thus flattening the boundary between the phases as function of μ_B . What makes this effect particularly interesting, in the context of results we have obtained, is the smoothness of the ratio P/ϵ at hadronization, which suggests a universal break up condition related to (hydrodynamic) flow.

D. Our hadronization boundary and its interpretation

The above two effects, the change in the location of the static phase boundary in presence of chemical equilibrium and the dynamics of collective matter flow toward breakup condition, are both non-negligible but hard to evaluate quantitatively. We believe that they can explain why the chemical freeze-out conditions T and μ_B are as presented in figure 5.

Our chemical freeze-out conditions are better shown in the T - μ_B plane, see figure 11. Considering results shown in figure 5, we are able to assign to each point in the T - μ_B plane the associate value of $\sqrt{s_{NN}}$. The RHIC dN/dy results are to outer left. They are followed by RHIC and SPS $N_{4\pi}$ results. The dip corresponds to the 30 and 40 AGeV SPS results. The top right is the lowest 20 AGeV SPS and top 11.6 AGeV AGS energy range. We see that the chemical freeze-out temperature T rises for the two lowest reaction energies 11.6 and 20 A GeV to near the Hagedorn temperature, $T = 160$ MeV. Such phase structure is discussed in the context of chiral quark pairing [10].

The size of error bars, in figure 11, is output of the fit process, and when it is rather large, it implies that the resulting χ^2 profile was relatively flat, or/and that there were two neighboring good fit minima. To guide the eye, we have added two lines connecting the fit results. As seen in figure 11, at $\mu_B = 0$, we find that hadronization occurs at $T = 140$ decreasing to $T = 120$ MeV at $\mu_B = 400$ MeV. Along this line $\gamma_q > 1.6$. As argued in the previous subsection IV C, due to the overpopulation of the quark phase space, we believe that this line is a true 1st order phase boundary between over-saturated hadron and quark matter.

There are at least two interpretations we can attempt

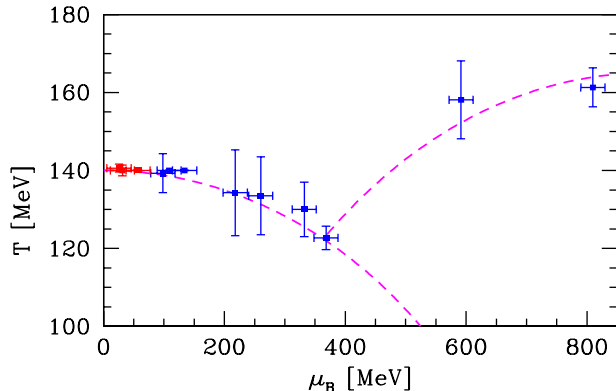


FIG. 11: T - μ_B plane with points obtained in the SHM fit. See text for discussion.

to understand the other branch in figure 11, the rise from $T \simeq 120$ to 160 for $\mu_B > 400$, which is accompanied by the sudden decrease of the phase space occupancy. Most ‘natural’ is to imagine that the dissolution of color bonds did not occur in heavy ion collisions below 30 A GeV, we are dealing with dense ‘conventional’ hadron matter. The colliding hadron system breaks up at higher temperature, which is a consistent freeze-out scenario for under-saturated hadron phase space. The under-saturation occurs since there was no time to make hadrons, i.e., chemical equilibration was not achieved.

Considering the kinetic scattering freeze-out condition, we see that, a high T , freeze-out for $\gamma_i < 0.5$ is consistent. The nucleon density scales with γ_q^3 and pion density with γ_q^2 . Therefore the dominant pion–nucleon scattering length scales as $L \propto 1/\gamma^5$, and this implies that, as the system expands, it freezes out at a higher T . Even so, the system size we found, see, e.g., the volume size in the fit results, in table I, is considerable suggesting a quite different expansion history of hadron matter which undergoes hadronization at high $m\mu_B, T$.

However, this rather standard picture of a conventional hadron matter formation at reaction energies below the transition point at $6.26 \text{ GeV} < \sqrt{s_{\text{NN}}^{\text{ST}}} < 7.61 \text{ GeV}$ may not be the valid explanation of results of our analysis. Namely, if the reaction history since first contact is different for the two reaction energy ranges, one would expect that the systematics of the final state entropy production, strangeness production, and strange antibaryon production has a visible break at the critical point. What we have shown is instead that these quantities show a rather smooth undisrupted rise with reaction energy. This means that the the initial conditions reached in the reaction where, e.g., entropy and strangeness are produced, is not undergoing a sudden change. The change occurs at the end near to the hadronization of matter. For this reason, we see a change in particle yields (the horn), statistical parameters jump, and the physical conditions at hadronization jump even more. The yields

of quantities which are driven by physics of initial dense matter formation (e.g., entropy content, strangeness content) change smoothly with heavy ion reaction energy in the domain we explored.

Moreover, even at the final stage, we do not see a hadron fireball breakup into free-streaming hadrons. We are swayed away from hadronic gas being the form of matter at breakup below $\sqrt{s_{\text{NN}}^{\text{ST}}}$ by the strange antibaryon production systematics we discussed in figure 4. We are searching thus for an explanation in terms of a new phase of matter, but clearly this cannot be the semi-perturbative quark–gluon plasma state.

The conceivable explanation of the fit result below 30 A GeV is presence, at the high baryon density arising at large μ_B , of a constituent quark plasma [60]. Even if the perturbative QCD quark phase is reached at high temperature, in expansion-cooling the system encounters the valon (word derived from ‘valance’ quark) phase in which the color quark bonds are broken, but chiral symmetry restoration is not completed, with quarks of mass $m_{u,d} \simeq 340 \text{ MeV}$ and $m_s \simeq 500 \text{ MeV}$ being the only active degrees of freedom. This scenario is not inconsistent with the finding on the lattice, that, for $\mu_B \rightarrow 0$ and in chemical equilibrium, the chiral symmetry restoration coincides with deconfinement transition.

In a valon matter, the number of quark pairs at temperature near to $T = 160 \text{ MeV}$ would be, considering the high constituent quark mass, even assuming chemical equilibrium, rather small. In breakup of this system, a relatively small γ_i^{HG} is achieved. Furthermore, since the mass of these constituent quarks is greater than that of the pion, the phase transformation between hadron and valon matter occurs at relatively large T , one can think of the pion with its low mass related greater pressure as pushing the transition boundary to higher T . Strangeness and importantly the entropy content in this phase arise due to prior perturbative QGP phase and hence such a valon system must be larger in volume. However, it is also conceivable that a fireball evolving fully in the valon phase would maintain much of the continuity we saw in hadronic observables. For example, u, d -valon-quark scattering can produce strange valon-quark pairs, and these give rise in hadronization to the abundances of strange antibaryons, as expected in the deconfined phase.

E. Final remarks

In summary, we have performed a complete analysis of the energy dependence of hadron production in heavy ion collisions, spanning the range beginning at the top AGS energy, to the top RHIC energy. We have made extensive predictions about particle production in the entire energy range. Among most interesting results is the finding that the best energy to search for the elusive pentaquark would be at SPS at 30 A GeV, where we find that the total yield is already fully developed, and the maximum of the ratio $\Theta^+(1540)/K_S \simeq 0.2$ is at 30 A

GeV, and is decreasing with increasing reaction energy. Of course, this finding presupposes existence of the exotic state. We have presented hadron yields important in the understanding of dilepton spectra.

We have shown that the threshold in energy which generates a horn in the K^+/π^+ yield ratio can be associated with the chemical freeze-out shifting rather rapidly toward condition of greatly increased hadronization densities. This transition separates the high entropy phase at high heavy ion reaction energy from a low entropy phase. This behavior parallels the findings for impact parameter dependence of RHIC results, where the low entropy phase is seen for small reaction volumes present at large impact parameters [3].

Several observables, including strangeness production, show continuity across the energy threshold at $6.26 \text{ GeV} < \sqrt{s_{NN}^{CT}} < 7.61 \text{ GeV}$, thus, it seems that the critical conditions expresses a change in the nature of the fireball breakup, and to a lesser degree a reaction energy dependent change in the nature of initial conditions reached in the reaction.

We have discussed, in depth, our findings about the hadronization condition $T(\mu_B)$ and have argued that at high reaction energies a 1st order phase transition is arising in the chemically non-equilibrated hot hadronic matter system. Detailed discussion was presented about possible changes in phases of hadronic matter as function of reaction energy and reaction volume.

Acknowledgments

We thank Marek Gaździcki for communication of data tables of NA49 results and for very valuable comments about the initial draft of this manuscript. We thank V. Friese for kind help with the NA49 ϕ -results. Work supported in part by a grant from: the U.S. Department of Energy DE-FG02-04ER4131. LPTHE, Univ. Paris 6 et 7 is: Unité mixte de Recherche du CNRS, UMR7589.

-
- [1] B. Muller, “Hadronic signals of deconfinement at RHIC,” [arXiv:nucl-th/0404015]; K. Adcox *et al.* [PHENIX Collaboration], “Formation of dense partonic matter in relativistic nucleus nucleus collisions at RHIC: Experimental evaluation by the PHENIX collaboration,” [arXiv:nucl-ex/0410003]; J. Adams *et al.* [STAR Collaboration], “Experimental and theoretical challenges in the search for the quark gluon plasma: The STAR collaboration’s critical assessment of the evidence from RHIC collisions,” [arXiv:nucl-ex/0501009].
- [2] M. Gaździcki *et al.* [NA49 Collaboration], *J. Phys. G* **30**, S701 (2004) .
- [3] J. Rafelski, J. Letessier and G. Torrieri, “Central-ity dependence of bulk fireball properties at RHIC,” [arXiv:nucl-th/0412072].
- [4] J. Rafelski and B. Müller, *Phys. Rev. Lett.* **48**, 1066 (1982) [Erratum-ibid. **56**, 2334 (1986)].
- [5] N. K. Glendenning and J. Rafelski, *Phys. Rev. C* **31**, 823 (1985); note that in Fig. 2 the pion yield from resonance decays is not included, this dilutes the expected yields by about factor two, flattening the curve.
- [6] J. Letessier, A. Tounsi, U. W. Heinz, J. Sollfrank and J. Rafelski, *Phys. Rev. Lett.* **70**, 3530 (1993), and *Phys. Rev. D* **51**, 3408 (1995) .
- [7] P. Koch, B. Muller and J. Rafelski, *Phys. Rept.* **142**, 167 (1986).
- [8] P. Koch and J. Rafelski, *Nucl. Phys. A* **444**, 678 (1985).
- [9] J. Rafelski and M. Danos, *Perspectives In High-Energy Nuclear Collisions*, NBSIR-83-2725 and GSI-83-6, see section 5, KEK scan available at http://ccdb3fs.kek.jp/cgi-bin/img_index?200031578; update: *Lecture Notes in Physics*, **231**, 361 (1985) (Springer-Verlag, Berlin); M. Danos and J. Rafelski, *Heavy Ion Phys.* **14**, 97 (2001) (M. Danos memorial volume).
- [10] M. Kitazawa, T. Koide, T. Kunihiro and Y. Nemoto, *Phys. Rev. D* **65**, 091504 (2002) .
- [11] M. Gaździcki, *Acta Phys. Polon. B* **34** (2003) 5771; M. Gaździcki and M. I. Gorenstein, *Acta Phys. Polon. B* **30**, 2705 (1999) .
- [12] G. Torrieri and J. Rafelski, *J. Phys. G* **30**, S557 (2004) .
- [13] G. Torrieri, W. Broniowski, W. Florkowski, J. Letessier and J. Rafelski, “SHARE: Statistical hadronization with resonances,” *Computer Phys. Comm. in press*, arXiv:nucl-th/0404083, and references therein by the authors.
- [14] J. Letessier and J. Rafelski, *Int. J. Mod. Phys. E* **9**, 107, (2000), arXiv:nucl-th/0003014
- [15] P. Koch, J. Rafelski and W. Greiner, *Phys. Lett. B* **123**, 151 (1983).
- [16] I. G. Bearden *et al.* [BRAHMS Collaboration], *Phys. Rev. Lett.* **90**, 102301 (2003).
- [17] F. Becattini, J. Cleymans, A. Keranen, E. Suhonen and K. Redlich, *Phys. Rev. C* **64**, 024901 (2001) .
- [18] J. Letessier, J. Rafelski and G. Torrieri, “Deconfinement energy threshold: Analysis of hadron yields at 11.6-A-GeV,” [arXiv:nucl-th/0411047].
- [19] M. Gaździcki, Commented compilation of NA49 results, private communication.
- [20] V. Friese *et al.* [The NA49 Collaboration], *J. Phys. G* **30**, S119 (2004) .
- [21] J. Rafelski and J. Letessier, *Acta Phys. Polon. B* **34**, 5791 (2003); and *J. Phys. G* **30** (2004) S1 .
- [22] B. B. Back *et al.* [E917 Collaboration], *Phys. Rev. C* **69**, 054901 (2004) .
- [23] J. Cleymans, H. Oeschler, K. Redlich and S. Wheaton “The horn and the thermal model,” [arXiv:hep-ph/0411187].
- [24] J. Letessier, G. Torrieri, S. Steinke and J. Rafelski, *Phys. Rev. C* **68**, 061901 (2003) .
- [25] V. Friese [NA49 Collaboration], *Nucl. Phys. A* **698**, 487 (2002).
- [26] J. Rafelski, J. Letessier and G. Torrieri, *Phys. Rev. C* **64**,

- 054907 (2001) [Erratum-ibid. C **65**, 069902 (2002)] .
- [27] J. Cleymans and K. Redlich, Phys. Rev. C **60**, 054908 (1999) .
- [28] S. S. Adler *et al.* [PHENIX Collaboration], Phys. Rev. C **69**, 034909 (2004) .
- [29] C. Markert [STAR Collaboration], J. Phys. G **30**, S1313 (2004) .
- [30] H. B. Zhang [STAR Collaboration], “Delta, K* and rho resonance production and their probing of freeze-out dynamics at RHIC,” [arXiv:nucl-ex/0403010]; J. Adams [STAR Collaboration], “K(892)* Resonance Production in Au+Au and p+p Collisions at $\sqrt{s_{NN}} = 200$ GeV at STAR,” [arXiv:nucl-ex/0412019], Submitted to Phys. Rev. C.
- [31] J. Adams *et al.* [STAR Collaboration], “Phi meson production in Au + Au and p + p collisions at $s^{*(1/2)} = 200$ -GeV,” Phys. Lett. B in press, [arXiv:nucl-ex/0406003].
- [32] G. Torrieri *et al.*, “Resonance Production in Heavy Ion Collisions at RHIC-200” manuscript in preparation.
- [33] C. Adler *et al.* [STAR Collaboration], Phys. Rev. Lett. **89**, 092301 (2002) .
- [34] K. Adcox *et al.* [PHENIX Collaboration], Phys. Rev. Lett. **89**, 092302 (2002) .
- [35] C. Adler *et al.*, Phys. Rev. C **65**, 041901 (2002).
- [36] C. Adler *et al.* [STAR Collaboration], Phys. Rev. C **66**, 061901 (2002) .
- [37] C. Adler *et al.* [STAR Collaboration], Phys. Lett. B **595**, 143 (2004) .
- [38] J. Adams *et al.* [STAR Collaboration], Phys. Lett. B **567**, 167 (2003) .
- [39] K. Adcox *et al.* [PHENIX Collaboration], Phys. Rev. C **69**, 024904 (2004) .
- [40] J. Adams *et al.* [STAR Collaboration], Phys. Rev. Lett. **92**, 182301 (2004) .
- [41] D. Elia [NA57 Collaboration], J. Phys. G **31**, S135 (2005).
- [42] I. G. Bearden *et al.* [BRAHMS Collaboration], “Charged meson rapidity distributions in central Au + Au collisions at $s(NN)^{(1/2)} = 200$ -GeV,” arXiv:nucl-ex/0403050.
- [43] B. B. Back *et al.*, Phys. Rev. Lett. **91**, 052303 (2003) .
- [44] I. G. Bearden *et al.* [BRAHMS Collaboration], Phys. Rev. Lett. **93**, 102301 (2004) .
- [45] J. I. Kapusta and S. M. H. Wong, Phys. Rev. Lett. **86**, 4251 (2001) .
- [46] G. E. Bruno [NA57 Collaboration], J. Phys. G **30**, S717 (2004) .
- [47] J. Rafelski, Phys. Rept. **88**, 331 (1982).
- [48] J. Letessier, A. Tounsi and J. Rafelski, Phys. Lett. B **389** (1996) 586.
- [49] J. Rafelski and J. Letessier, Phys. Lett. B **469**, 12 (1999).
- [50] Z. Fodor and S. D. Katz, JHEP **0404**, 050 (2004), .and references therein.
- [51] C. R. Allton *et al.*, Phys. Rev. D **66**, 074507 (2002) .
- [52] J. Rafelski and J. Letessier, Nucl. Phys. A **702**, 304 (2002) .
- [53] P. Braun-Munzinger, K. Redlich and J. Stachel, arXiv:nucl-th/0304013, in Quark Gluon Plasma 3, eds. R.C. Hwa and Xin-Nian Wang, World Scientific Publishing, and references therein.
- [54] A. Peikert, F. Karsch, E. Laermann and B. Sturm, Nucl. Phys. Proc. Suppl. **73**, 468 (1999) .
- [55] C. Bernard *et al.* [MILC Collaboration], Phys. Rev. D **71**, 034504 (2005) .
- [56] C. R. Allton, S. Ejiri, S. J. Hands, O. Kaczmarek, F. Karsch, E. Laermann and C. Schmidt, Phys. Rev. D **68**, 014507 (2003) .
- [57] H. Z. Huang and J. Rafelski, “Hadronization and quark probes of deconfinement at RHIC,” arXiv:hep-ph/0501187.
- [58] T. Csorgo and J. Zimanyi, Heavy Ion Phys. **17**, 281 (2003) .
- [59] J. Rafelski and J. Letessier, Phys. Rev. Lett. **85**, 4695 (2000) .
- [60] I. I. Roizen, E. L. Feinberg and O. D. Chernavskaya, Phys. Usp. **47**, 427 (2004) [Usp. Fiz. Nauk **47**, 427 (2004)] .